Chemical Science

ROYAL SOCIETY OF CHEMISTRY

REVIEW

View Article Online
View Journal | View Issue

Check for updates

Cite this: *Chem. Sci.*, 2025, **16**, 3788

Noble-metal-free catalysts for the oxygen evolution reaction in acids

Junwei Han,[a] Qian Liu,[a] Yue Yang[a] and Hao Bin Wu *[ab]

Oxygen evolution catalysts are critical components of proton exchange membrane water electrolysers (PEMWEs), playing a decisive role in determining both the performance and cost of these devices. Non-noble metal-based oxygen evolution catalysts have recently drawn significant attention as potential alternatives to expensive noble metal catalysts. This review systematically summarizes the mechanism of non-noble metal catalysts for the oxygen evolution reaction in acids with respect to their activity and stability, incorporating theoretical calculations and the Pourbaix diagram. Advanced *in situ* techniques are highlighted as powerful tools for probing intermediate evolution and valence changes and further elucidating the catalytic mechanism. Furthermore, key strategies for enhancing catalytic activity and durability, such as elemental doping, the support effect, surface protection and novel phase design, are discussed. Finally, this review provides insights into the remaining challenges and emerging opportunities for advancing practical oxygen evolution catalysts in PEMWEs.

Received 11th December 2024
Accepted 5th February 2025

DOI: 10.1039/d4sc08400d

rsc.li/chemical-science

Open Access Article. Published on 05 February 2025. Downloaded on 2/13/2026 4:26:31 AM.
This article is licensed under a Creative Commons Attribution-NonCommercial 3.0 Unported Licence.

1. Introduction

In light of the growing global energy demand and the depletion of conventional energy sources, the world is now confronted with a significant challenge—the development of sustainable energy.[1] Hydrogen energy possesses various advantages including high energy density and zero emissions, which enables large-scale and environmentally friendly utilization.[2] Compared with other hydrogen production methods such as photolysis, gas reformation and biomass gasification, water electrolysis has gained significant attention for its cleanliness, compactness, and flexibility.[3] Noteworthily, a proton exchange membrane water electrolyser (PEMWE) operating under acidic conditions shows advantages of high H_2 purity and high current density compared to other electrolysers.[4] Meanwhile, the anodic four-electron-transfer OER exhibits sluggish kinetics in a H^+ concentrated environment. Considering the local acidic environment resulting from the use of a perfluorosulfonic acid (PFAS) membrane, a PEMWE places higher demands on the acid resistance of an anode catalyst.[5] Hence, developing highly active and stable OER catalysts has become an urgent need for large-scale application of the PEMWE.[6]

Among the OER catalysts for PEMWEs, IrO_2 (ref. 7 and 8) and RuO_2 (ref. 9–11) present ultra-high activity and decent stability for the OER under acidic conditions, and are yet limited by the scarcity and high cost of noble metal resources. Therefore, the exploration of noble metal-free catalysts for acidic OER has gained significant attention.[12,13] Numerous noble metal-free alternatives have been proposed, including transition metal oxides,[14] nitrides,[15] phosphides,[16] sulfides,[17] and other complex compounds (such as polyoxometalates,[18] phosphates,[19] and metal–organic frameworks[20]). Compared with noble metal catalysts, it is even more challenging to achieve both high activity and durability for noble metal-free OER catalysts.[21] Despite some promising candidates and modification strategies reported so far, systematic and comprehensive guidance for the development of high-performance acidic OER catalysts has not been well established.[22] Thanks to the rapid advances in computational materials science, high-throughput material screening that points out future directions has become possible.[23]

In this review, we summarize the development of OER catalysts operating under acidic conditions, which could potentially be used for PEMWEs and other related applications. Starting from the mechanism, this review introduces the widely accepted adsorbate evolution mechanism (AEM) and lattice oxygen mechanism (LOM), as well as the nascent oxide path mechanism (OPM) and proton donor–acceptor mechanism (PDAM). Then, by incorporating high-throughput computational approaches, the calculated Pourbaix diagrams provide guidance for the screening of acid-stable catalysts within the anodic potential window. Advanced *in situ* characterization methods as powerful tools to analyze the catalytically active sites and the reaction mechanism have also been summarized. On the basis of mechanism analysis and theoretical calculations, experimental strategies to develop advanced noble metal-free catalysts for acidic OER are classified, such as elemental

[a]*School of Materials Science and Engineering, Zhejiang University, Hangzhou 310027, China*

[b]*State Key Laboratory of Silicon and Advanced Semiconductor Materials, Zhejiang University, Hangzhou 310027, China. E-mail: hbwu@zju.edu.cn*

© 2025 The Author(s). Published by the Royal Society of Chemistry

Open Access Article. Published on 05 February 2025. Downloaded on 2/13/2026 4:26:31 AM. This article is licensed under a Creative Commons Attribution-NonCommercial 3.0 Unported Licence.

doping, the support effect, surface protection and new phase design, especially in cobalt- and manganese-based oxide systems. Finally, bottlenecks and future directions in the search for highly active and durable noble metal-free catalysts are discussed.

2. Proton exchange membrane water electrolyzers, thermodynamics, Pourbaix diagrams and *in situ*/*operando* techniques

First, the basic structure and challenges of proton exchange membrane water electrolyzers (PEMWEs) are introduced. The traditional thermodynamic mechanisms of the OER on the oxide surface include the AEM and LOM, while alternative mechanisms such as the OPM and PDAM have been proposed recently. In addition, the Pourbaix diagram is widely adopted to explain the catalyst stability during the OER in acids. Along with these theoretical approaches, *in situ*/*operando* characterization techniques are indispensable to reveal the evolution of catalytically active sites and shed light on the microscopic reaction mechanism.

2.1 Proton exchange membrane water electrolysers

The basic structure of PEMWEs is the membrane electrode assembly (MEA) connected in between monopolar/bipolar plates.[24] The MEA is the core component of PEMWEs where the electrochemical reactions (OER/HER) occur, while monopolar/bipolar plates carry current/heat and transport reactants/products from MEA.[25] The MEA is an assembled stack of two electrodes and a proton exchange membrane, and the catalyst layers are generally coated on both sides of the membrane and sandwiched between two porous transport layers (PTLs). The choices of PTLs are typically platinized titanium felt for the anode and carbon paper for the cathode, allowing facile liquid/gas transport and electrical connection.[26] Such a design helps to mitigate the energy penalties related to electronic/ionic conduction and mass transport, resulting in rapid electrochemical reactions at high current density.

For the PEMWE system, the deviation of the cell voltage from the thermodynamic value originates from three sources: the activation overpotentials from electrochemical reactions, ohmic overpotentials associated with proton and electron conduction, and concentration overpotential due to mass transport limitation.[27–29] The polarization of anodic reactions (OER) represents a major source of the voltage penalty due to the sluggish four-electron water oxidation process.[30] In terms of the techno-economic consideration of PEMWEs, the Ir-based OER catalyst typically accounts for around 25% of the total cost of the MEA in commercial PEMWEs due to its high cost (~174 $ per g, year of 2024) and high mass loading (~4–12 g m^{-2}).[31,32] Therefore, searching for highly active and low-cost acid OER catalysts has been a major task in the field.

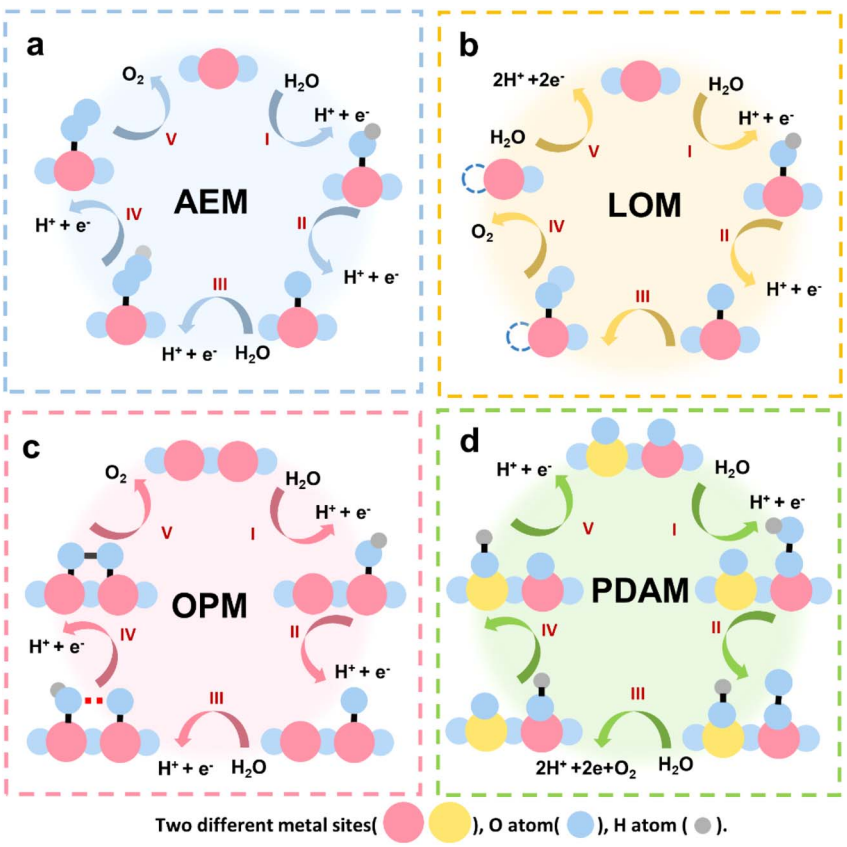

Fig. 1 Schematics of OER mechanisms: the (a) adsorbate evolution mechanism (AEM), (b) lattice oxygen mechanism (LOM), (c) oxide path mechanism (OPM), and (d) proton donor–acceptor mechanism (PDAM).

Open Access Article. Published on 05 February 2025. Downloaded on 2/13/2026 4:26:31 AM. This article is licensed under a Creative Commons Attribution-NonCommercial 3.0 Unported Licence.

2.2 Thermodynamic mechanism of the OER in acids

The AEM was originally proposed by Rossmeisl *et al.*,[33–36] who used density functional theory to calculate the binding energy of surface adsorbed intermediates as a criterion of catalyst activity. As shown in Fig. 1a, the AEM undergoes a proton–electron coupling process, involving three intermediates OH*, O*, and OOH* generated by the evolution of water molecules adsorbed at active centers. Specifically, in an acidic system, the water molecule is first adsorbed on the metal active site and undergoes a dehydrogenation step to produce the M–OH* species; the M–OH* species undergoes another dehydrogenation step to produce the M–O* species, which then binds to another water molecule to produce M–OOH* species; finally, another dehydrogenation reaction is carried out to finish the cycling with the breaking of the M–O bond and the release of O_2. However, according to the AEM theory, the binding energies of M–OH* and M–OOH* intermediates have been constrained by a scaling relationship. Specifically, the gap between the adsorption energies of OH* and OOH* is theoretically fixed as 3.2 eV, independent of the binding energy of M–O*, which provides an immutable overpotential of the OER catalysts obeying the AEM theory.[37] However, many catalysts have been experimentally observed to exhibit lower overpotentials that overcome the limit proposed by the AEM theory, suggesting alternative reaction pathways.[38] Meanwhile, in oxide-based catalyst systems,[39,40] the generation of surface lattice oxygen and oxygen vacancies provides a new perspective to explain the OER with higher activity, and thus the LOM was established.

The LOM is not thermodynamically favorable as it involves the breaking of surface lattice metal–oxygen bonds.[41] However, the involvement of lattice oxygen can be promoted by modulating the catalyst surface electronic structure and increasing the overlap between the 3d orbitals of metal and the 2p orbitals of oxygen.[42] As shown in Fig. 1b, a typical LOM undergoes a similar process to the AEM until the formation of M–O*. In the LOM pathway, M–O* species directly combine with lattice oxygen in the crystal structure to release O_2, generating an oxygen vacancy (V_O); subsequently, another H_2O molecule is adsorbed and deprotonated to fill the oxygen vacancy. The proposed LOM breaks the limitation caused by the scaling effect of OH* and OOH* species in the AEM and satisfactorily explains the experimentally observed enhanced catalytic activity. However, the involvement of lattice oxygen further induces the dissolution of transition metals and compromises the structural stability of catalysts.[43]

Overall, the LOM and AEM benefit the activity and stability of OER catalysts, respectively.[44] However, the above two mechanisms are not well adapted to catalysts with low overpotential and high stability, and thus the oxide path mechanism (OPM) and proton donor–acceptor mechanism (PDAM) have been recently proposed.[45] Unlike the AEM and LOM in which the electrooxidation of water molecules occurs at a single active site, the OPM and PDAM are based on the synergy of two adjoining catalytically active sites. The OPM (Fig. 1c) begins with water adsorption and dehydrogenation to produce an M–OH* intermediate, which is subjected to direct coupling with another M–OH* intermediate to produce O_2.[14] Catalysts with high density of metal active sites would theoretically benefit the OPM that involves the coupling step of two intermediates. Since the OPM does not involve the generation of M–OOH* intermediates, the typical scaling limitation in the AEM does not apply to the OPM, which potentially warrants the OER with a lower overpotential. In terms of stability, lattice oxygen does not participate in the OER through the OPM, which favors the stabilization of catalysts. Similar to the OPM, the PDAM (Fig. 1d) also relies on the formation of M–OO* intermediates. However, the two active centers in the PDAM are typically different atoms, with one serving as the primary reaction center and the other functioning as an indirect center to accept protons.[46] The PDAM emphasizes the asynchronous transfer of protons and electrons between these distinct active centers, often facilitated by electron modulation induced by oxygen or metal vacancies. Compared to the AEM and LOM, the OPM and PDAM theoretically promise OER catalysts with both high stability and intrinsic activity. However, how to design OER catalysts that catalyze water oxidation through a desirable mechanism and how to experimentally verify the reaction mechanisms remain key challenges in the field.

2.3 Stability of catalysts and the Pourbaix diagram

Most noble-metal-free OER catalysts are unstable in acidic electrolytes. Searching for potential catalysts with high stability under acidic OER conditions (*e.g.*, pH < 3 and potential > 1.23 V *vs.* RHE) has become the research priority.[47] The Pourbaix diagram, also known as a potential–pH diagram, is an electrochemical equilibrium diagram illustrating stable species or the equilibrium state of a system in a specific potential range and pH environment. The Pourbaix diagram can conveniently reflect the possibility of corrosion/dissolution of metals and metal compounds from a thermodynamic perspective, and is thus used to screen candidates as stable acidic OER catalysts.[48] Combining the Gibbs free energy gap (ΔG_{pbx}) under specific pH–potential conditions, the calculated band gap (E_g) for considering the electronic properties, and convex hull (E_{hull}) for estimating the phase stability, 68 possible acid-stable candidates for oxygen evolution were identified.[23]

Co-based and Mn-based oxides such as Co_3O_4 and MnO_2 are promising OER catalysts, which however exhibit distinct Pourbaix diagrams.[49] For Co_3O_4, the high potential and low pH range only allow the stable existence of Co^{2+} species,[50] and the stability under specific conditions can be regulated by introducing other elements to change the phase region distribution in the Pourbaix diagram. For example, the Pourbaix diagrams of La-modified and pristine Co_3O_4 (ref. 51) showed the pH–potential effect on the form of elements present on the surface and the hydroxyl stabilization effect. It is generally believed that Mn-based catalysts present better stability in acidic OER, attributed to the fact that MnO_2 can remain stable under pH < 2 conditions and in the 1.2 to 1.8 V potential window according to the Mn–H_2O Pourbaix diagram.[52] Nevertheless, as a thermodynamic steady-state methodology, the Pourbaix diagram cannot reflect the kinetic factors in acidic OER.

© 2025 The Author(s). Published by the Royal Society of Chemistry

Open Access Article. Published on 05 February 2025. Downloaded on 2/13/2026 4:26:31 AM.
This article is licensed under a Creative Commons Attribution-NonCommercial 3.0 Unported Licence.

The stability of non-noble metal catalysts has been a key challenge in the field, which is generally associated with dissolution of metal ions at high voltages. Although the Pourbaix diagram provides a thermodynamic prediction of stability, the degradation of catalysts is rather complicated, and is related to the catalytic mechanism and the structure of catalysts. Several strategies have been proposed to improve the stability of acidic OER catalysts, including the enhancement of metal–oxygen bonding, interfacial protection, crystallinity design, *etc.*[49] Moreover, catalysts may exhibit different degradation behaviors in MEA-based electrolyzers compared to liquid electrochemical cells. Therefore, effective performance assessment protocols are highly needed to bridge the gap between in-lab catalyst development and practical application scenarios.

2.4 *In situ* and *operando* characterization techniques

Monitoring catalyst evolution during electrochemical reactions is of great importance to understand the catalytic mechanisms, which relies on various characterization techniques.[53,54] *Ex situ* techniques analyze the difference between pre- and post-reaction samples, while *in situ* techniques monitor real-time reaction processes. Notably, real-time monitoring of structure changes[55] and reaction intermediates[56] can be accomplished by *in situ*/*operando* characterization techniques. Compared with *in situ* techniques that provide on-site monitoring under specific reaction conditions, *operando* techniques focus on real-time monitoring during the reaction. Several *in situ* and *operando* characterization techniques have been widely used in the studies of the OER, such as synchrotron X-ray absorption spectroscopy (XAS), Raman spectroscopy, Fourier-transform infrared spectroscopy (FTIR) and differential electrochemical mass spectrometry (DEMS), dedicated to determine the true active species and reaction intermediates.[57]

Raman spectroscopy is based on the Raman scattering phenomenon. During the Raman measurement, a small fraction of incident laser photons experience inelastic scattering and transfer energy to the tested sample, leading to vibrational or rotational transitions of chemical bonds.[58] The frequency gap between scattered light and incident light known as a Raman shift is related to many chemical characteristics such as molecular structures, chemical bonding and lattice vibration.[59] By measuring the Raman shift and intensity of Raman scattered light, species transformation and interfacial evolution during electrochemical reactions can be monitored in real time. Raman spectroscopy can not only detect the behavior of water molecules,[55] but also the formation of metal–oxygen bonds[14] at low chemical shifts during the catalytic process. Taking the Raman spectrum of Co_3O_4 as an example, typical Raman peaks at 480 cm^{-1} (E_g), 520 cm^{-1} (F_{2g}), 620 cm^{-1} (F_{2g}), and 690 cm^{-1} (A_{1g}) can be probed. During an *in situ* Raman measurement, the full width at half maximum (FWHM) of the A_{1g} peak increases with operating time, attributed to the formation of an amorphous hydrated layer on the surface of Co_3O_4 that hinders the focusing of the laser light.[60] The characteristic Raman peaks of Co_3O_4 can also be seen in the composite of Co_3O_4/CeO_2.[61] As the potential increased, another Raman signal at 600 cm^{-1} attributed to CoOOH species can be observed at 1.2 V (*vs.* RHE) and gradually disappears after reaching the OER onset potential (Fig. 2a). Meanwhile, the A_{1g} Raman peak was found to be red-shifted after reaching the OER onset potential, which was ascribed to Co^{4+} species (Fig. 2b). Thus, the *in situ* Raman spectroscopy measurement suggests that high-valence Co species rather than CoOOH might be the catalytically active species for acidic OER.

Raman spectroscopy has been used to study various cobalt oxide-based OER catalysts. The Raman spectrum of Ba-doped Co_3O_4 ($Co_{3-x}Ba_xO_4$) showed a peak at 456 cm^{-1} at 1.45 V (*vs.* RHE), attributed to the formation of OH* on the surface.[14] Liu *et al.*[56] investigated a CeO_2-loaded $CoNiPO_x$ ($CeO_2/Co_2NiP_{0.03}O_x$) hetero-structured catalyst using Raman spectroscopy, which exhibited two weak peaks at 465 and 525 cm^{-1} at 1.2 V (*vs.* RHE), ascribed to O–Ce–O and Co^{II}–O bonds, respectively. Compared with $Co_2NiP_{0.03}O_x$, $CeO_2/Co_2NiP_{0.03}O_x$ manifested the Co^{III}–O bonding signal at a lower potential of 1.2 V (*vs.* RHE), suggesting a transition from Co^{II} to Co^{III} during acidic OER. In addition to Co_3O_4, CoO_2 is also proved to be active during acidic OER and stable at high potential according to the Pourbaix diagram. Zhang *et al.*[63] prepared Co loaded MnO_2 by reacting MnO_2 with molten cobalt salt and tested it in an electrolyte containing Co^{2+} to ensure the stable deposition of CoO_2 during electrolysis. The 90-Co–MnO_2 catalyst was characterized by *in situ* Raman spectroscopy over a potential range of 0 to 1.8 V (*vs.* RHE) in 0.1 M $HClO_4$ containing 2.4 mg per mL Co^{2+}. Two peaks corresponding to MnO_2 were observed at 624 cm^{-1} and 579 cm^{-1}, and a peak associated with CoOOH was observed at 497.8 cm^{-1} within the potential range of 1.2–1.7 V (*vs.* RHE). CoOOH was then converted to CoO_2 above 1.7 V, as indicated by the peak at 460.9 cm^{-1}. Although *in situ* Raman spectroscopy enables the real-time monitoring of the evolutionary process during operation, the weak signal intensity of intermediates highlights the need for advanced spectroscopic techniques with higher detection sensitivity, such as surface-enhanced Raman spectroscopy (SERS), tip-enhanced Raman spectroscopy (TERS), *etc.*[64]

X-ray absorption spectroscopy (XAS) is a characterization technique based on the interaction of materials and high-energy X-rays, such as those generated by synchrotron light sources[65] (Fig. 2c). By analyzing the scattering, absorption and emission phenomena, detailed information about the local atomic arrangement can be obtained, including bond lengths, coordination numbers and so on. When the X-ray energy matches the binding energy of electrons in the irradiated sample, resonance absorption occurs, causing a sudden increase in X-ray absorption, referred to as the adsorption edge. This adsorption edge gives rise to the X-ray absorption near edge structure (XANES), which provides insights into the electronic configuration and local atomic structure around the absorbing centers. XANES allows determination of valence states, d-band properties, orbital hybridization, symmetry, and other structural information. At higher X-ray energies, absorbing-center electrons are excited to continuum states, creating wave interference patterns known as extended X-ray absorption fine structures (EXAFS), providing information on

Open Access Article. Published on 05 February 2025. Downloaded on 2/13/2026 4:26:31 AM.
This article is licensed under a Creative Commons Attribution-NonCommercial 3.0 Unported Licence.

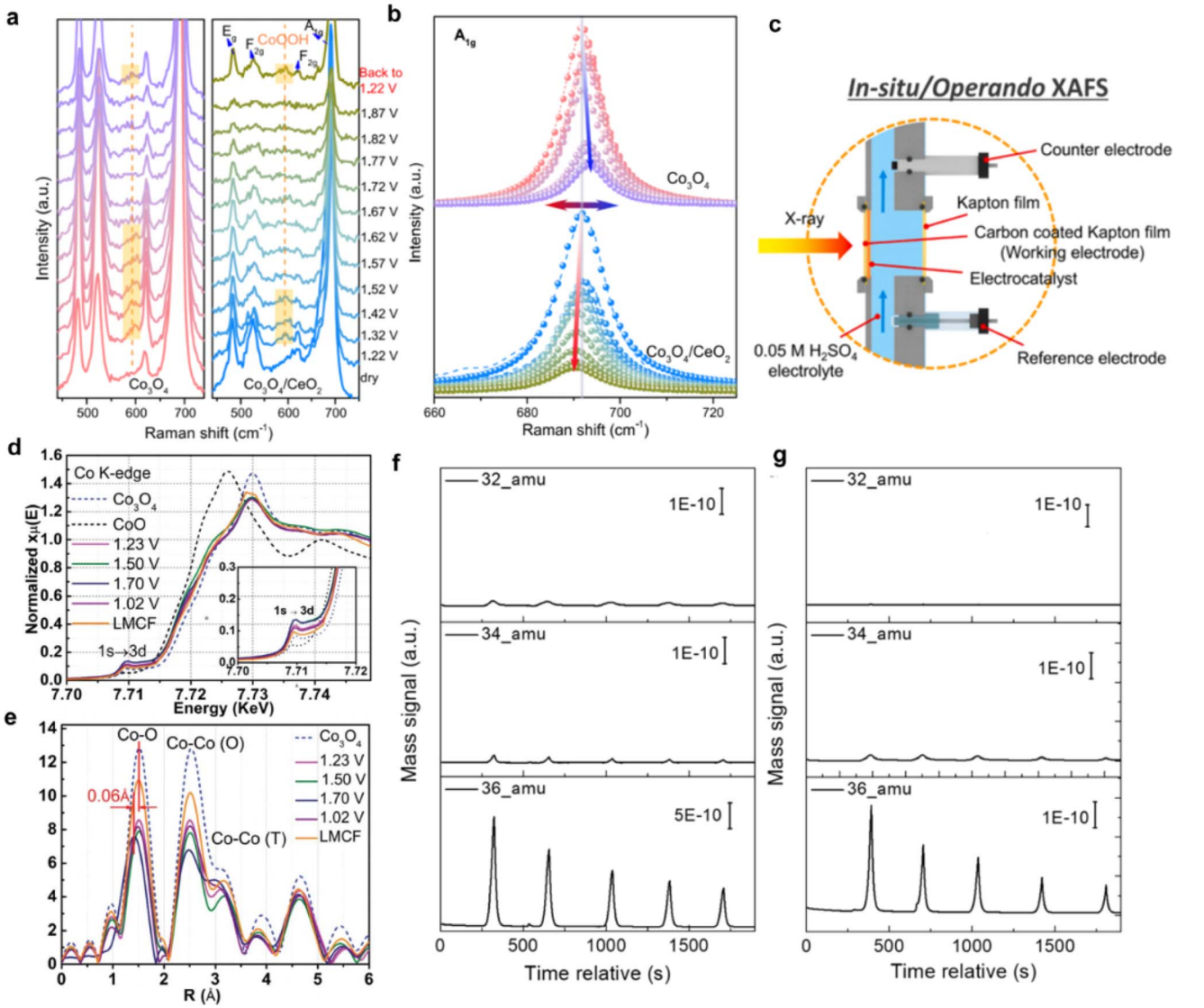

Fig. 2 (a) *In situ* Raman spectra and (b) Raman A_{1g} peaks of Co_3O_4 and Co_3O_4/CeO_2 at various constant potentials (*vs.* RHE). Reproduced with permission.[61] Copyright 2021, Springer Nature. (c) Scheme of an *in situ* XAS instrument. Reproduced with permission.[62] Copyright 2023, Elsevier. (d) Fluorescence XANES spectra and (e) *R*-space EXAFS spectra collected at the Co K-edge. Reproduced with permission.[51] Copyright 2023, The American Association for the Advancement of Science. *Operando* differential electrochemical mass spectrometry signals of O_2 products for (f) $Co_{3-x}Ba_xO_4$ and (g) Co_3O_4. Reproduced with permission.[14] Copyright 2023, American Chemical Society.

the local atomic arrangement and coordination numbers surrounding the absorbing centers.

Chong *et al.*[51] investigated a self-supported LaMn-doped ZIF-67 fiber (LMCF) catalyst using XAS. *In situ* XANES of the Co K-edge showed a slight red-shift and reduced intensity as the potential increased, indicating a lower oxidation state in LMCF with a smaller O coordination number (Fig. 2d). At the same time, the enhanced intensity of the 1s–3d orbital transition peak suggests a less symmetric coordination environment for cobalt of LMCF, verifying oxide lattice distortion caused by oxygen vacancies in the lattice structure (Fig. 2e). The higher white line intensity of La in LMCF than that of La_2O_3 suggests a higher coordination number of La in LMCF. Similarly, Wang *et al.*[62] analyzed the structural stability of $FeCoSbO_x$ using the *in situ* XAS technique. They observed that the Co pre-edge intensity of $FeCoO_x$ increased with higher potentials, whereas that of $FeCoSbO_x$ remained almost unchanged up to 1.8 V (*vs.* RHE). This suggests that Sb doping alleviated structural distortion during operation.

In situ differential electrochemical mass spectrometry (DEMS) utilizes mass spectrometry to identify species with different *m*/*z* ratios and their relative abundances, providing insights into reaction intermediates and pathways.[66] For example, when evaluating Ba-doped Co_3O_4 in $H_2{}^{18}O$ and $H_2{}^{16}O$ electrolytes, $Co_{3-x}Ba_xO_4$ consistently produced $^{32}O_2$, $^{34}O_2$, and $^{36}O_2$ during each LSV cycle (Fig. 2f), while Co_3O_4 produced only $^{34}O_2$ and $^{36}O_2$ (Fig. 2g), supporting the proposed OPM mechanism.[14]

Advancements in advanced spectroscopy and analytical techniques have significantly enhanced the ability to explore reaction intermediates, active sites and real-time reaction

© 2025 The Author(s). Published by the Royal Society of Chemistry

Open Access Article. Published on 05 February 2025. Downloaded on 2/13/2026 4:26:31 AM. This article is licensed under a Creative Commons Attribution-NonCommercial 3.0 Unported Licence.

pathways in catalytic reactions. *In situ* Raman spectroscopy is mainly applied to detect chemical structure changes on electrode surfaces during reactions, and is particularly sensitive to oxygen reaction intermediates. *In situ* XAS collects bulk information of the catalysts and reflects changes in the overall valence state and coordination environment. *In situ* DEMS provides real-time monitoring of ion dissolution, offering experimental information for catalyst failure analysis. The combination of various *in situ* characterization techniques is essential for providing a comprehensive understanding of the catalytic process. Nevertheless, experimental confirmation of the catalytic mechanism with both high spatial and temporal resolution remains highly challenging. Therefore, developing *in situ*/*operando* techniques is essential for monitoring critical intermediates, understanding the reaction processes, and further elucidating the acidic OER catalytic mechanism.

3. Transition metal oxides as OER catalysts in acids

First-row d-block metal oxides, especially Co and Mn oxides, have been widely investigated as promising noble-metal-free OER catalysts. The intrinsic activity and catalyst evolution of Co-based and Mn-based oxides as acid OER catalysts with various modification methods, such as atomic doping, the support effect, protection coating and phase design, have been studied.

3.1 Co-based oxides

3.1.1 Intrinsic activity and catalyst evolution. With the trend of developing noble-metal-free catalysts for acidic oxygen evolution, Co-based oxides with high activity, decent durability, and cost-effectiveness have gained much attention from researchers.[13] Typically, spinel Co_3O_4 is considered one of the most promising anode catalysts for acid water electrolysis with a comparable OER overpotential to state-of-the-art IrO_2 (ref. 12) (Fig. 3a). However, the insufficient stability of Co_3O_4 associated with cobalt ion dissolution at high potentials severely hampers its practical applications.

Determining the surface structure of the catalyst under operating conditions is the key to analyze the catalytic activity. A recent study by Zhang *et al.*[38] investigated the vacancy-induced effect on the evolution of Co_3O_4 during the oxygen evolution process by constructing Co and O vacancies. Co_3O_4 undergoes

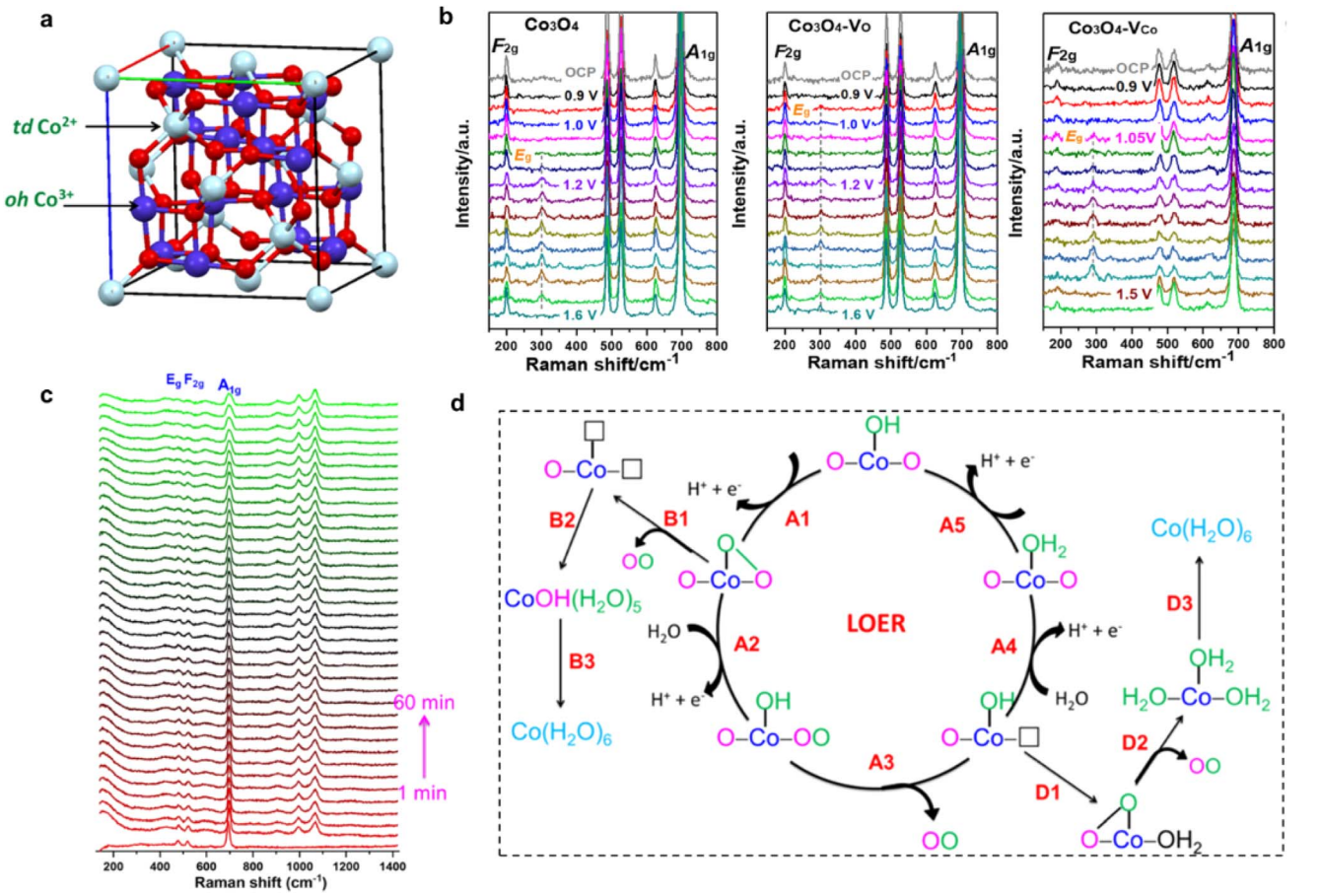

Fig. 3 (a) Crystal structure of Co_3O_4. Reproduced with permission.[60] Copyright 2021, American Chemical Society. (b) *In situ* Raman spectra of Co_3O_4, Co_3O_4-V_O and Co_3O_4-V_{Co} in the voltage window from 0.9 to 1.55/1.6 V (*vs.* RHE). Reproduced with permission.[38] Copyright 2023, American Chemical Society. (c) Time-resolved *in situ* confocal Raman spectra of Co_3O_4 at 1.72 V (*vs.* RHE) and (d) the LOER mechanism and the degradation route of Co_3O_4 during LOER. Reproduced with permission.[60] Copyright 2021, American Chemical Society.

Open Access Article. Published on 05 February 2025. Downloaded on 2/13/2026 4:26:31 AM. This article is licensed under a Creative Commons Attribution-NonCommercial 3.0 Unported Licence.

a two-step reconstruction during the OER process, from oxide to a hydroxide analogue and then to an oxyhydroxide analogue, which is accompanied by adsorption of hydroxyl and deprotonation. The potentials at which the E_g peaks appear or disappear in Raman spectroscopy demonstrate the difference in hydroxyl adsorption and deprotonation capacities of various structures. It has been found that O vacancies lead to easier hydroxyl adsorption and Co vacancies lead to easier deprotonation (Fig. 3b). Moreover, Co vacancies contribute to a shorter Co–Co distance, which show the highest OER activity.

Similar to studies on the alkaline OER, Natarajan *et al.*[60] synthesized Co_3O_4 with different types of defects and investigated the reconstruction of surface hydrous oxide layers under acidic conditions. Their findings showed that Co_3O_4 with higher crystallinity tends to form a thinner hydrous oxide layer during the OER. By *in situ* Raman analysis (Fig. 3c), the hydrous oxide layer thickens with operation time, and a direct correlation was also found between the ratio of Co(III)/Co(VI) and layer thickness. However, a thick surface hydrous oxide layer does not promote the catalytic activity but leads to the deactivation of the catalyst due to the loss of contact and degradation of active surface sites. The dissolution of Co species is closely linked to the LOM. This suggests that with the formation of oxygen vacancies around the metal sites, H_2O would possibly occupy the oxygen vacancies and form soluble high-valent Co hydrates (Fig. 3d).

Another important issue is the effects of an acidic environment on catalyst stability and activity. The study by Huang *et al.*[61] shed light on this issue by testing the Co_3O_4 and Co_3O_4/CeO_2 catalysts in H_2SO_4 solutions with different pH values. LSV curves show that the catalyst activity is less impacted by the concentration of protons. Therefore, when developing OER catalysts for acidic systems, stability might be the first consideration rather than activity. Over the past decade, many studies have provided insights into stability issues[67] in view of the degradation mechanism, and various strategies have been conducted including atomic doping, constructing heterostructures, surface engineering and phase design. The following sections will focus on the modulation of Co_3O_4 catalysts to improve catalyst activity and stability.

3.1.2 Atomic doping. Atomic doping is a facile method to form lattice distortions and vacancy defects, which lead to lattice structure alterations or changes in the electronic structure of the active center.[68] Considering properties of dopants such as lattice matching, atomic structure, ionic radius and valence, potential dopants of Co_3O_4 include transition metals such as Fe,[69] Ni,[70] and Mn[71,72] and non-metallic elements such as N[73] and P.[56,74] Doping Co_3O_4 with large size elements such as lanthanide elements becomes difficult due to the mismatch of the ionic radius, yet the enrichment of dopants on the particle surface might still provide a certain degree of acid resistance.[51]

Nwanebu *et al.*[70] prepared Ni_xCo_{1-x}–oxide catalysts on titanium plates by direct nitrate pyrolysis and investigated the effects of Ni/Co ratio on the catalytic OER performance. When the Ni molar percentage was lower than 50%, the crystal structure was dominated by the Co_3O_4 phase, and *vice versa* by the NiO phase. Meanwhile, the catalytic performance showed a volcano distribution since Ni doping induces the formation of high-valence active Co species whereas excessive Ni results in NiO with low OER activity. Wang *et al.*[14] synthesized a Ba-doped Co_3O_4 catalyst ($Co_{3-x}Ba_xO_4$) through facile electrodeposition and heat treatment, which exhibited an overpotential of 278 mV at 10 mA cm^{-2} in 0.5 M H_2SO_4 (Fig. 4a) and stable operation for over 110 h. Through Ba doping, the Co–Co bond length was shortened, creating conditions for direct dehydrogenation O–O coupling (Fig. 4b). The *in situ* synchrotron FT infrared (FTIR) spectra directly detected the generation of O–O bonds, which is consistent with the oxygen bridge intermediate in the OPM (Fig. 4c). DFT calculations showed that the O–O coupling step was considered as the rate determining step which promoted the OPM pathway under acidic conditions. Chong *et al.*[51] synthesized a Mn/La co-doped Co_3O_4 fiber catalyst (LMCF) using zeolitic imidazolate frameworks (ZIF-67) as a precursor through electrospinning and annealing treatment. The doping of Mn cations inside the ZIF lattice triggered a higher valence of Co active sites and shorter Co–Co band length, which contribute to promoted acidic oxygen evolution activity. Meanwhile, the La cations with strong affinity to *OH groups concentrated at the surface of cobalt oxide, provide excellent acid-proof ability (Fig. 4d). The Pourbaix diagrams of different crystal planes such as (111), (110) and (100) in La-modified and pristine Co_3O_4 were calculated and compared as shown in Fig. 4e. Among the five regions, regions I and II contain La ions, so the structure is unstable and soluble. Regions III, IV, and V exhibit relative stability due to the presence of Co^{2+}, Co^{3+}, and La^{3+} surfaces connected with OH*, OOH*, and O*. The LMCF catalyst was evaluated in a PEMWE under potentiostatic conditions, demonstrating stable operation over 100 h at a cell voltage of 1.65 V (Fig. 4f). Doping Co_3O_4 with Fe[69] and Ag[75] has also been proven to improve the catalytic activity and durability of acidic OER.

Doping Co oxides with non-metal elements such as carbon, nitrogen, sulfur and phosphorus would have profound effects on the catalytic activity and stability. Yang and co-workers[73] demonstrated nanostructured Co_3O_4/CN deposited on carbon paper as a self-standing electrode using ZIF-67 as a precursor. FT-EXAFS shows that Co–O/N was established in the Co_3O_4/CN structure and the doping of N induced O vacancies by partially replacing lattice oxygen. In addition, the nitrogen-doped carbon structure improves the acid resistance of Co_3O_4, which guarantees stability for 80 h at 10 mA cm^{-2} in 0.5 M H_2SO_4. Shang *et al.*[74] used the solvothermal method to introduce P into the Co_3O_4 lattice, where P^{5+} replaces Co^{3+} located in the 16d sites with an octahedral coordination. The unique PO_6 units increased the percentage of Co^{2+} in the Co_3O_4 lattice, which suppresses the leaching of Co ions and increases the stability during acidic OER.

3.1.3 Support and coating effects. Supports might have profound effects on tuning the electronic properties of the catalysts, and could be used to optimize the catalytic activity and stability. Metal oxides with acid resistance, intermediate affinity and strong valence bonds have been used as catalyst supports for acidic OER, including CeO_2,[56] TiO_2,[76] PbO_2,[77] PdO,[78] ZnO[79] and Sb-doped SnO_2.[80] Huang *et al.*[61] prepared CeO_2

© 2025 The Author(s). Published by the Royal Society of Chemistry

Open Access Article. Published on 05 February 2025. Downloaded on 2/13/2026 4:26:31 AM.
This article is licensed under a Creative Commons Attribution-NonCommercial 3.0 Unported Licence.

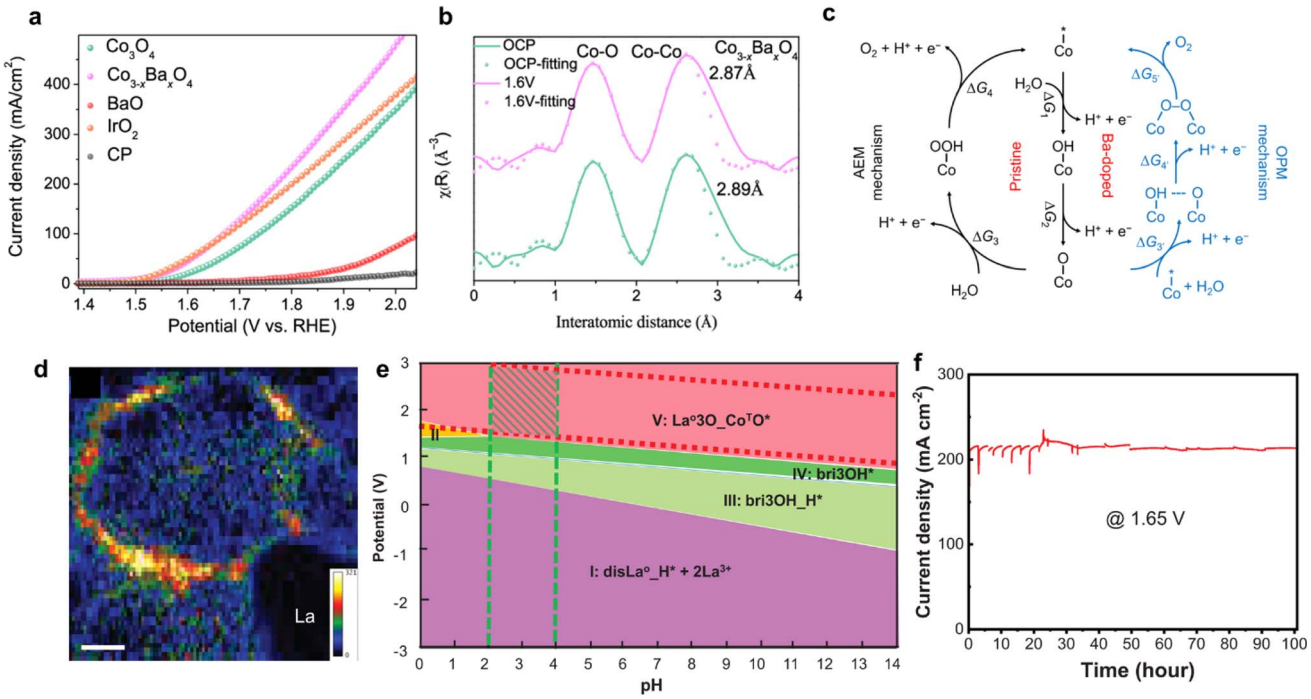

Fig. 4 (a) LSV and (b) *in situ* EXAFS spectra of the Co K-edge of $Co_{3-x}Ba_xO_4$ and (c) the OPM *vs.* the AEM for catalysts in acidic electrolytes. Reproduced with permission.[14] Copyright 2023, American Chemical Society. (d) STEM image and the corresponding La distributions (scale bar, 2 nm) of LMCF and the surface (e) Pourbaix diagram for the La-doped Co_3O_4 (111) facet obtained from the DFT+*U* calculations. (f) Potentiostatic measurement of a PEMWE using the LMCF catalyst at 1.65 V. Reproduced with permission.[51] Copyright 2023, The American Association for the Advancement of Science.

nanosheets loaded with Co_3O_4 nanoparticles, where rapid electron transfer was expected at the interfaces between CeO_2 and Co_3O_4 to avoid charge accumulation at the catalytic sites. CeO_2 might benefit the formation of high valence active cobalt as suggested by *in situ* Raman characterization. Kinetic isotope effect (KIE) analysis indicates that the OER is less sensitive to the proton concentration in the electrolyte, which is consistent with the LSV curves in electrolytes with different pH values.

Constructing a protective surface layer has been another widely used strategy to mitigate the performance degradation caused by catalyst detachment as well as direct proton attack on metal–oxygen bonding in strong acidic environments.[81] Carbon coatings, especially highly graphitized carbon, have been considered as preferred choices due to their high conductivity, decent stability and convenient preparation, despite the possible corrosion at high potential. Lai *et al.*[82] prepared carbon protected Co_3O_4 by spraying cobalt nitrate on carbon paper with a gas diffusion layer fixed on a hot plate. The carbon coated Co_3O_4 catalyst achieved an overpotential of 460 mV for more than 80 hours in 0.5 M H_2SO_4. Yang *et al.*[83] also reported a Co_3O_4 catalyst with a 3.5 nm thick carbon layer, synthesized using glucose as the carbon source. LSV curves demonstrated the negative impact of the carbon layer on catalytic activity, with the overpotential increased by 150 mV. However, the durability of the catalyst improved, with the duration time extending by 20% to 86.8 h at 10 mA cm^{-2}. The incorporation of carbon into electrocatalysts or electrodes might also modulate hydrophobicity, which could help to prevent excessive solvation of metal oxides, thus minimizing their dissolution. For example, Yu *et al.*[84] synthesized a nano-Co_3O_4@C composite, and introduced graphite and paraffin oil during electrode preparation. This process created partially hydrophobic zones that effectively suppressed the dissolution of active Co_3O_4.

Apart from carbon coating, acid stable metal oxides such as TiO_2 (ref. 76) and F doped tin oxide (FTO)[85] have also been investigated as coating materials. Tran-Phu *et al.*[76] explored the effect of a TiO_2 coating layer on the catalytic properties of Co_3O_4. Coating layers with a suitable thickness would contain pitting channels, which maintain a balance between protection and exposure of the catalytic surface. Yeh *et al.*[85] synthesized FTO coated and loaded Co_3O_4 samples with a low Co^{3+}/Co^{2+} ratio and oxygen vacancies, exhibiting enhanced stability.

Selection of materials with good electrical conductivity, acid resistance and mechanical strength is critical for effective coating strategies. However, achieving both high acid resistance and electrical conductivity is challenging due to the limitation of intrinsic properties of available materials. As a result, catalysts designed through coating strategies often require compromises in catalytic activity. Thus, maintaining both catalytic activity and stability presents a significant challenge in these approaches. Besides, the structure and OER mechanism of the active sites at the coating interface remains unclear and requires further investigation.

3.1.4 Phase design. Spinel Co_3O_4 consists of repeating octahedral and tetrahedral units. By incorporating second or third elements, a variety of dual- or multi-component catalysts

Open Access Article. Published on 05 February 2025. Downloaded on 2/13/2026 4:26:31 AM. This article is licensed under a Creative Commons Attribution-NonCommercial 3.0 Unported Licence.

with diverse structures have been developed, such as spinel and rutile structures.[86] For acidic OER catalysts requiring enhanced stability, elements with strong metal–oxygen bonds and lattice matching properties are preferred, such as Ti,[87] Mn,[72] Sb,[88] Fe,[89] Pb,[89,90] *etc.* Anantharaj *et al.*[87] prepared spinel Co_2TiO_4 by a co-precipitation method, achieving an overpotential of 513 mV in 0.5 M H_2SO_4 at a current density of 10 mA cm^{-2}. The synthesis of Co_2TiO_4 was significantly influenced by the sintering temperature. When the sintering temperature was below 900 °C, only the Co_3O_4 phase was observed, suggesting that the formation of Co_3O_4 hinders the crystallization of Ti oxides. After the stability test, Raman peaks near 200–400 cm^{-1} almost completely disappeared, indicating that surface Co_2TiO_4 had transformed into the Co_3O_4 phase. SAED analysis revealed the presence of Co_3O_4 on the post-test Co_2TiO_4 surface. XPS analysis indicated that the Co^{3+}/Co^{2+} ratio on the surface increased from 0.327 to 0.561, with strong O_{1s} peaks attributed to the surface Co_3O_4.

According to the Pourbaix diagram, Sb_2O_5 is an acid-resistant and potential-endurance oxide that can help stabilize active centers in an acidic medium during the OER.[91] As a result, introducing Sb into Co-oxide systems as a stabilizer can extend the stability of catalysts. However, the poor electrical conductivity of metal–oxide catalysts may diminish the catalytic performance. Evans *et al.*[92] synthesized rutile $CoSb_2O_6$ *via* electrodeposition, demonstrating stability for over 24 h at a current density of 10 mA cm^{-2} in 0.5 M H_2SO_4. Wang *et al.*[91] synthesized pyrochloryl $Co_2Sb_2O_7$, which exhibited an ultra-low overpotential of 288 mV and stability for over 40 h at 1 mA cm^{-2}. After the constant potential test, the XRD pattern showed peaks corresponding to tetragonal $CoSb_2O_6$, indicating the transformation of $Co_2Sb_2O_7$ into $CoSb_2O_6$ during the OER process. The evolved $CoSb_2O_6$ acted as a stable protective layer to improve the stability.

However, the introduction of Ni into the $CoSb_2O_x$ system did not improve the performance, though the reasons have not been thoroughly discussed.[88] Wang *et al.*[62] prepared $FeCoSbO_x$ catalysts on nickel foam *via* direct pyrolysis, reducing the onset potential by 271 mV at a current density of 10 mA cm^{-2} compared with that of FeO_x prepared by the same method

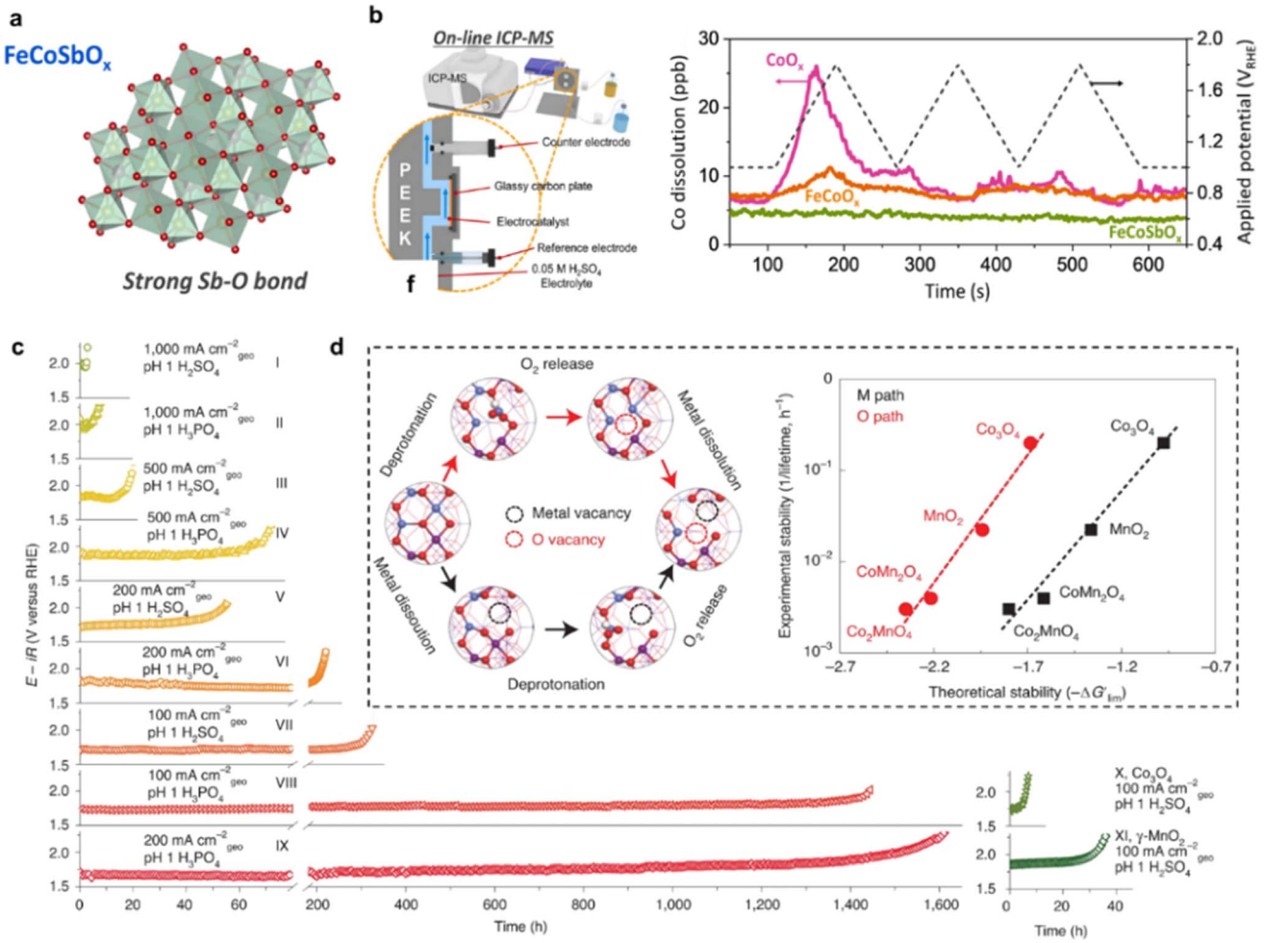

Fig. 5 (a) Scheme of the crystal structure of $FeCoSbO_x$. (b) Scheme of *in situ*/*operando* ICP-MS analysis and Co dissolution profiles during cyclic voltammetry conducted by using an on-line ICP-MS. Reproduced with permission.[62] Copyright 2023, Elsevier. (c) Long-term stability of Co_2MnO_4 during the OER in acid. (d) Two possible pathways of dissolution and correlation between experimental and theoretical stability. Reproduced with permission.[71] Copyright 2022, Springer Nature.

© 2025 The Author(s). Published by the Royal Society of Chemistry

Open Access Article. Published on 05 February 2025. Downloaded on 2/13/2026 4:26:31 AM. This article is licensed under a Creative Commons Attribution-NonCommercial 3.0 Unported Licence.

(Fig. 5a). The *in situ* ICP-MS test revealed that Co dissolution of $FeCoSbO_x$ was significantly suppressed (Fig. 5b). X-ray absorption near-edge structure (XANES) spectral analysis indicated that Fe maintained a stable electronic structure, while the Co K-edge XANES peaks for CoO_x, $FeCoO_x$ and $FeCoSbO_x$ electrodes shifted toward higher photon energies. The pre-edge peak, which represents structural symmetry, shifted notably for $FeCoO_x$, whereas $FeCoSbO_x$ showed only a slight change. Overall, Sb contributed positively to structural symmetry and stability.

For inert components with poor conductivity, elements with catalytic activity and strong metal–oxygen bonds, such as Mn, are better choices for balancing stability and catalytic activity in acidic OER catalysts. Li *et al.*[71] designed a spinel Co/Mn oxide film (Co_2MnO_4) by pyrolyzing nitrate at 300 °C on an FTO support, achieving 200 mA cm^{-2} for over 2000 h in H_3PO_4 electrolyte with pH = 1 (Fig. 5c). Bader charge analysis revealed enhanced electron transfer from Mn to O on the Co_2MnO_4 surface, confirming the formation of stronger Mn–O bonds (Fig. 5d). Additionally, it is worth noting that the type of electrolyte can have a huge impact on stability, likely due to the effect of anion adsorption on the electrode surface. Notably, in phosphate electrolytes, the stability of Co-based catalysts was significantly enhanced according to previous studies. Therefore, further emphasis should be placed on the study of catalyst–electrolyte interfaces.

3.2 Mn-based oxides

Manganese-based oxides are characterized by rich valences and variable structures, such as MnO_2, Mn_2O_3, Mn_3O_4, *etc.*[93] According to the Pourbaix diagram of Mn–H_2O, MnO_2 is the most stable phase in the OER potential range under acidic conditions, which makes it a promising candidate for acidic OER.[49]

Differing superposition and connection of the basic repeating unit [MnO_6] results in structural variants of MnO_2,[94] such as cryptomelanes (α-MnO_2) with a 2 × 2 tunnel structure (Fig. 6a), pyrolusites (β-MnO_2) with a 1 × 1 tunnel structure (Fig. 6b), birnessites (δ-MnO_2) with a layered structure (Fig. 6c), and nsutite-type γ-MnO_2 (Fig. 6d) composed of 1 × 1 and 1 × 2 tunnels. Hayashi *et al.*[95] evaluated the OER activity of various MnO_2 (δ-MnO_2, α-MnO_2, γ-MnO_2, and β-MnO_2) and ranked their OER activity in PEMWEs as α-MnO_2 > β-MnO_2 > δ-MnO_2 > γ-MnO_2. This difference in activity may stem from the specific adsorption of intermediates within the different-sized tunnels formed by the distinct arrangement of [MnO_6] units. Kong *et al.*[98] synthesized MnO_2 by electrodepositing a manganese sulfate solution onto a Ti felt substrate and modulated the ratio of Mn–O structural units of the crystal structure through different heat treatment temperatures. As the heat treatment temperature increases, the proportion of planar oxygen increased, leading to enhanced catalyst stability. Pair distribution function analysis revealed that planar oxygen exhibits stronger Mn–O binding compared to pyramidal oxygen. This finding was also supported by DFT calculations, which showed that the dissolution from planar oxygen sites is energetically less favorable than that from pyramidal oxygen sites.

Further studies have identified the high-spin electron configuration of Mn^{3+} as a critical active species that facilitates the formation and transformation of unstable Mn–O intermediate bonds. Yan *et al.*[99] reported that the use of ionic liquid additives can induce the phase transition from β-MnO_2 to α-MnO_2, leading to alterations in both phase composition and morphology. TEM, EDX, and FTIR analyses collectively showed that the surface of α-MnO_2 is coated with ionic liquid cations, which further adsorb anions, such as OH^-. In contrast to Mn 2p, the analysis of Mn 3s peak splitting (ΔE_{3s}) provides a more accurate characterization of the Mn^{n+} valence state. The peak area revealed a higher Mn^{3+}/Mn^{4+} ratio in the ionic liquid-modified α-MnO_2. Other than the impact of ionic liquid additives, variations in electrodeposition procedures might also affect the transformation of MnO_2 during electrocatalysis. δ-MnO_2 deposited *via* constant potential was transformed into the α-Mn_3O_4 phase after cathodization, and then into disordered δ-MnO_2 through a multi-step anodic oxidation or oxygen generation process, which exhibited enhanced activity.[100] XPS analysis shows a mixed Mn^{3+}/Mn^{4+} valence state in the disordered δ-MnO_2 phase, a result of defect generation during the spinel-to-layered structure conversion that stabilizes Mn^{3+}. Li *et al.*[101] employed the stochastic surface walking (SSW) pathway sampling method to elucidate the atomic-level mechanism underlying the transformation from α-Mn_3O_4 into δ-MnO_2, and validated the role of defects in the phase transformation process through theoretical calculations. Li *et al.*[96] investigated the stabilization voltage window of γ-MnO_2 under acidic conditions, demonstrating that the catalyst dissolves into MnO_4^- when the voltage exceeds the stabilization voltage window. UV/vis absorption spectra showed that Mn^{3+} formed at 1.4 V during positive voltage sweeps, which catalyzed the onset of the OER at 1.6 V *vs.* RHE. As the potential reached 1.8 V, MnO_4^- was detected, suggesting that the dissolution of γ-MnO_2 mainly produces MnO_4^- (Fig. 6e). Consequently, a stabilization window between 1.6 V and 1.75 V was established for γ-MnO_2 during acidic OER. γ-MnO_2 exhibited stability for over 1800 h at 10 mA cm^{-2} and 1.73 V, whereas the stability decreased to only 120 h at 100 mA cm^{-2} and 1.8 V.

The introduction of halogen atoms is an effective strategy to enhance the metallic bond strength and regulate the electronic structure of the active centers. By substituting oxygen atoms in MnO_2 with halogen ions, such as F,[102,103] Cl,[97] or Br,[97] halogen–Mn bonds are formed, which not only shift the d-band center but also create a stronger metallic bond with improved stability. Patel *et al.*[103] prepared crystalline F-doped $Cu_{1.5}Mn_{1.5}O_4$ nanoparticles by adding $CuCl_2$ and NH_4F to amorphous MnO_2. A linear downshift of the d-band center was achieved with increasing F-doping, which improved the overall electrochemical catalytic activity. Ghadge *et al.*[102] observed that fluorine doping in $Mn_{0.8}Nb_{0.2}O_2$ induced a positive shift in the Nb 3d and Mn 2p peaks, corresponding to the formation of high-valence active sites. Lemoine *et al.*[104] prepared a hydrated MnFe fluoride and found that the dehydrated $MnFeF_{4.6}O_{0.2}$ with an amorphous structure showed remarkable stability under highly acidic conditions. Pan *et al.*[97] prepared a manganese oxybromide catalyst *via* pyrolysis of manganese bromide, achieving

Open Access Article. Published on 05 February 2025. Downloaded on 2/13/2026 4:26:31 AM.
This article is licensed under a Creative Commons Attribution-NonCommercial 3.0 Unported Licence.

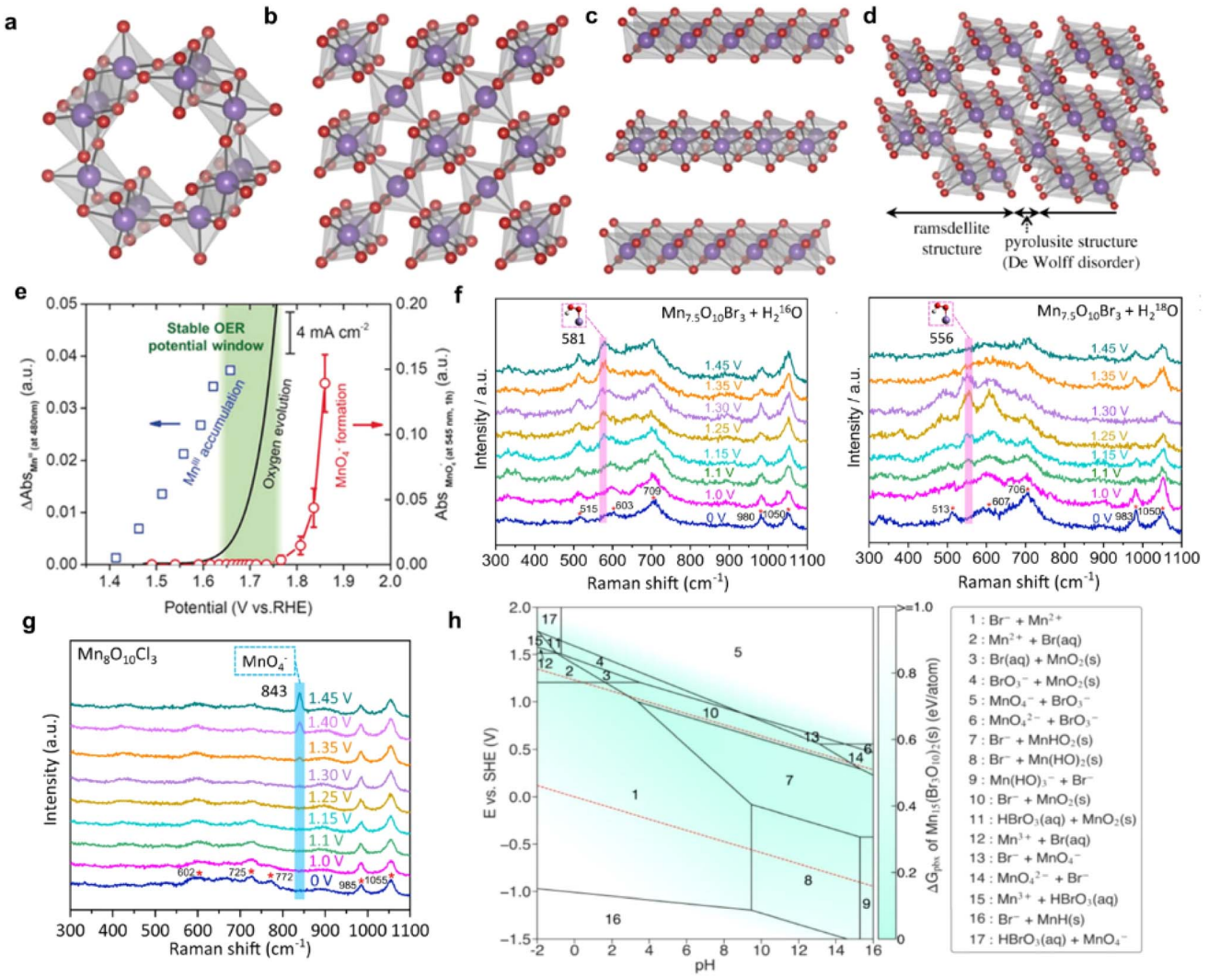

Fig. 6 Structure of (a) α-MnO_2, (b) β-MnO_2, (c) δ-MnO_2 and (d) γ-MnO_2. Reproduced with permission.[95] Copyright 2019, Royal Society. (e) Potential dependence of Mn^{3+} accumulation, oxygen evolution current, and MnO_4^- generation of γ-MnO_2. Reproduced with permission.[96] Copyright 2019, Wiley-VCH. *In situ* Raman spectra of (f) $Mn_{7.5}O_{10}Br_3$ and (g) $Mn_8O_{10}Cl_3$. Reproduced with permission.[97] Copyright 2022, Springer Nature. (h) Calculated Mn–O–Br Pourbaix diagrams generated with an aqueous ion concentration of 10^{-4} M at 25 °C. Reproduced with permission.[97] Copyright 2022, Springer Nature.

an OER overpotential of 295 mV at 10 mA cm^{-2} and stability for over 500 h. Comparative studies of halogen doping effects revealed notable differences. Isotopic analysis in $H_2{}^{16}O$ and $H_2{}^{18}O$ electrolytes showed a negative shift of 26 cm^{-1} at 1.25 V, indicating that the Mn–$^{18}O^{18}OH$ intermediate is produced by the exchange of two ^{16}O atoms (Fig. 6f). Raman spectroscopy of $Mn_8O_{10}Cl_3$ displayed a distinct MnO_4^- peak at 843 cm^{-1} after reaching 1.35 V (*vs.* RHE), indicating catalyst degradation through the formation of MnO_4^- (Fig. 6g). $Mn_{7.5}O_{10}Br_3$ and $Mn_8O_{10}Cl_3$ can be stabilized by forming a MnO_x (*e.g.*, MnO_2) passivation layer on the surface at potentials of 1.40–1.60 V (*vs.* RHE) under acidic conditions (pH = 0) (Fig. 6h).

Another common modification strategy involves incorporating inert, acid-resistant components into MnO_2, such as PbO_2,[105,106] TiO_2,[107] and SiO_2.[108] However, this strategy typically reduces catalytic performance due to the poor electrical conductivity and non-catalytic nature of these acid-resistant substances. Fryfendal *et al.*[107] prepared a multilayer MnO_2 catalyst with surface-modified TiO_2 by sputtering deposition and predicted the catalyst lifetime by a mass loss method. At 1.8 V, the expected lifetime of MnO_2 was 140 h, whereas TiO_2-modified MnO_2 extended this to 265 hours. Directly combining acid-resistant elements with catalytically active elements to form new phases, rather than heterogeneous structures, has proven to be a superior modification method. For example, Moreno-Hernandez *et al.*[109] synthesized a NiMnSb ternary rutile oxide that exhibited a stability of 168 h at 10 mA cm^{-2} due to the synergistic effect of the Ni–Mn elements and the stabilizing effect of Sb during acidic OER. Zhou *et al.*[110] explored the origin of the catalytic activity in the rutile phase Mn–Sb–O and demonstrated that the Mn–Sb–O system stabilizes Mn^{3+}. XPS results showed that the Mn valence remained between +2 and

© 2025 The Author(s). Published by the Royal Society of Chemistry

Open Access Article. Published on 05 February 2025. Downloaded on 2/13/2026 4:26:31 AM. This article is licensed under a Creative Commons Attribution-NonCommercial 3.0 Unported Licence.

+3. Interestingly, increasing the Mn content in the Mn–Sb–O system elevated the valence state of Mn while that of Sb remained unchanged, suggesting that abundant Mn may facilitate the formation of oxygen vacancies or covalent Mn–O bonding. Ifkovits *et al.*[111] coupled the OER with the Ce^{4+}/Ce^{3+} redox reaction in the $Mn_ySb_{1-y}O_x$ system and found a similar correlation between Mn^{3+} concentration and catalytic activity in the Mn-rich system, with Tafel slopes up to 100 mV dec^{-1}. Furthermore, an inverse relationship between catalytic activity and stability with increasing Sb content was observed.

4. Transition metal nitrides, sulfides and phosphides

In addition to oxides, transition metal nitrides, sulfides, and phosphides have also been considered as acidic OER catalysts with optimized electronic structures and acidic stability. Note that transition metal carbides[112] have been generally considered unstable during acidic OER due to carbon corrosion. Lei *et al.*[113] developed a self-supported iron nitride catalyst loaded on polyaniline-electrodeposited exfoliated graphene (FeN_4/NF/EG) and explored the effect of different annealing temperatures on catalytic performance. Polyaniline provided attachment sites for the loaded iron nitride and also exhibited oxygen evolution activity. The catalyst stayed stable at a current density of 20 mA cm^{-2} for more than 24 h, which was attributed to the enhanced conductivity from graphitic N and highly active catalytic sites induced by pyridine N. Nitridation often modifies the valence states of active metal sites. Liu *et al.*[114] synthesized a NiCo–nitride/oxide catalyst forming a heterogeneous structure between a NiCo–nitride shell and a NiCo–oxide core by annealing $NiCo_2O_4$ in an NH_3 atmosphere. XPS analysis showed negative shifts in the binding energy peaks of Ni 2p and Co 2p, indicating decreased valence states of Ni and Co after nitridation. Additionally, nitridation enhances metallic bonding and produces stronger Co–Co/Ni–Ni bonds, thus enhancing corrosion-resistant ability. Besides boosting catalytic activity, nitridation also serves as a protective coating for supports such as Ti mesh and carbon paper. Guo *et al.*[15] developed an OER catalyst operated across a wide pH range by constructing Co_xN nanoparticles on TiN coated titanium mesh by atomic layer deposition (ALD) (Fig. 7a). Co_xN and TiN evolved into an active and protective CoTi layered double hydroxide, contributing to the long-term stability. The catalyst required only 398 mV overpotential to achieve a current density of 50 mA cm^{-2} in 1 M $HClO_4$.

Transition metal sulfides also show great potential in the OER due to their unique electronic structure and diverse modulation methods. However, only a few sulfide-based OER catalysts under acidic conditions have been reported, such as CoS_2,[17] MoS_2 (ref. 116) and $Ni_4Fe_5S_8$.[117] Wu *et al.*[116] investigated the catalytic activity of MoS_2 with different crystalline phases and found that the octahedral 1T phase exhibited higher catalytic activity than the trigonal prismatic 2H phase. Meanwhile,

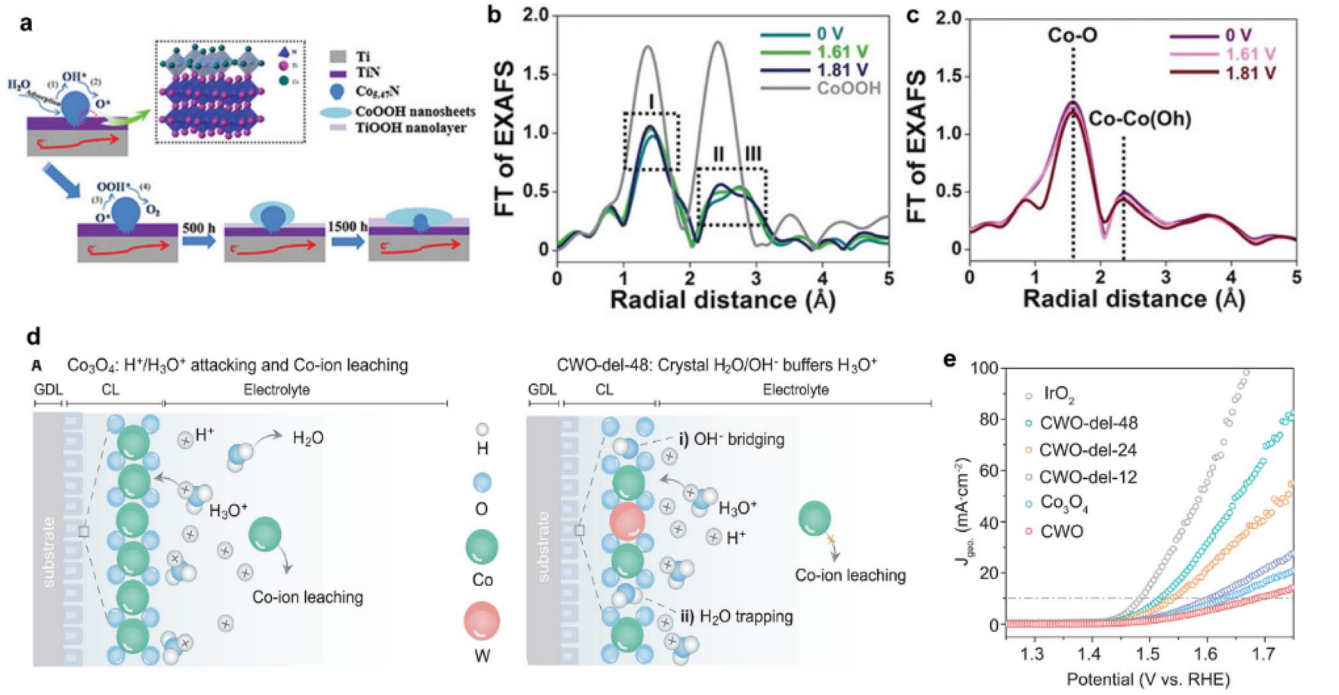

Fig. 7 (a) Proposed self-transformation of Ti/TiN @ $Co_{5.47}N$. Reproduced with permission.[15] Copyright 2020, Wiley-VCH. *Operando* Co K-edge extended X-ray absorption fine structure (EXAFS) spectra of (b) $Co_3(PO_4)_2$ and (c) $Co_3(PO_4)_2 \cdot 8H_2O$ at different potentials. Reproduced with permission.[19] Copyright 2020, Wiley-VCH. (d) Schematic illustration of the dissolution path of Co ions in Co_3O_4 and CWO-del-48. Reproduced with permission.[115] Copyright 2024, The American Association for the Advancement of Science. (e) Linear-sweep voltammetry of CWO-del-based catalysts at 5 mV s^{-1} in 0.5 M H_2SO_4 electrolyte. Reproduced with permission.[115] Copyright 2024, The American Association for the Advancement of Science.

Open Access Article. Published on 05 February 2025. Downloaded on 2/13/2026 4:26:31 AM. This article is licensed under a Creative Commons Attribution-NonCommercial 3.0 Unported Licence.

activation of 1T MoS_2 was observed during potential cycling between 1.2 V and 2.0 V, attributed to the rearrangement of MoS_2 nanosheets by oxygen molecules generated during the OER process, leading to better exposure of active sites. Heterogeneous structures formed between MoS_2 and other metal sulfides can modulate the valence states and promote the generation of high-valence active sites. For example, Yang *et al.*[17] grew Co_9S_8 and MoS_2 nanosheets on Ni_3S_2 nanorods as a bifunctional overall water splitting catalyst and found that the heterogeneous interface facilitated electron transfer through up shifting Co 2p binding energy and down shifting Mo 3d binding energy.

The choice of electrolyte such as phosphoric acid, sulfuric acid, or perchloric acid, greatly influences the stability of acidic OER catalysts, potentially due to different anion adsorption states at the reaction interface and catalyst evolution.[71] Therefore, the introduction of phosphorus could improve stability by forming phosphorus oxide at the interface. Liu *et al.*[118] prepared cobalt–manganese phosphide arrays grown on nickel phosphide nanoplates (CoMnP/Ni_2P nanosheet-based microplate arrays). The doping of Mn induced charge transfer from CoP to MnP, creating high-valent cobalt active centers. At the same time, the catalyst maintained superhydrophilic and supergasphobic characters, which mitigated the negative effect of gas bubbles on mass transfer at high current density. In addition to CoMnP/Ni_2P, NiFe based phosphide catalysts also showed good stability in acidic OER. Hu *et al.*[16] designed an amorphous NiFeP catalyst that maintained an overpotential of 540 mV for over 30 h in 0.05 M H_2SO_4 at 10 mA cm^{-2}.

5. Other transition metal compounds

Similar to noble metal molecular complexes, complex transition-metal compounds have been investigated for water oxidation in acidic media, including polyoxometalates[18,119,120] (POMs), MOF-supported catalysts,[20] cobalt phosphates[19,121,122] and cobalt tungstate.[115] However, practical application remains distant due to challenges such as limited conductivity, restricted current density and high overpotentials. Meanwhile, alloys containing acid stable elements, such as Ni_2Ta,[123] Fe_5Si_3,[124] Mn_5Si_3 (ref. 125) and $TiMn_2$,[126] might be candidates for acidic OER. Yet the electrochemical performance and structural evolution of these alloys have been poorly understood at this stage and need further studies.

Kanan *et al.*[127] developed an *in situ*-synthesized KCoPO amorphous film electrocatalyst with self-healing properties, prepared through electro-cycling in aqueous solution containing phosphoric acid and cobalt ions. This study demonstrated that an amorphous composite of cobalt and phosphoric ions would be a potential catalyst for the OER in strong acid. While insoluble cobalt phosphate salts with octahedral and tetrahedral sites have been studied, the catalytic mechanism of these two structures needs further exploration. Qi *et al.*[19] synthesized cobalt phosphate catalysts featuring either exclusively tetrahedral or octahedral sites, allowing for direct comparison of their catalytic performance. $Co_3(PO_4)_2$ with tetrahedral sites exhibits higher activity than its octahedral counterpart, attributed to the more facile formation of high valence (hydro)oxides on the dehydrated tetrahedral $Co_3(PO_4)_2$ surface. EXAFS analysis showed minimal change in the spectra of the octahedral cobalt phosphate at positive potentials, indicating the difficulty in forming high-valent active intermediates (Fig. 7b and c). This might be related to the six-coordination of cobalt atoms in octahedral cobalt phosphate, requiring ligand removal to form Co=O species. Ram *et al.*[115] prepared layered cobalt tungstate (CWO-del-48) by alkali etching of high-valent tungsten, a process that facilitates the incorporation of water and hydroxide at the surface, thereby mitigating the leaching of active cobalt during the reaction (Fig. 7d). The CWO-del-48 catalyst demonstrated an overpotential of 288 mV at 10 mA cm^{-2} and maintained stable operation at 1 A cm^{-2} for over 600 h in a PEMWE (Fig. 7e).

Polyoxometalates (POMs), composed of oxygen-rich ligands coordinated with metal cations, offer several advantages, including acid resistance, structural tunability and ease of synthesis. The introduction of different cations into POM systems has tremendous effects on their properties, and elements such as Fe,[120] Ba and Cs[18] have been explored. Blasco-Ahicart *et al.*[18] found that introducing barium ions into $[Co_9(H_2O)_6(OH)_3(HPO_4)_2(PW_9O_{34})_3]^{16-}$ (Co-POM) remarkably enhances the OER performance by exposing more active sites. 40% Ba[Co-POM] exhibits an overpotential of 361 mV at 10 mA cm^{-2} in 1 M H_2SO_4, outperforming the noble-metal catalyst IrO_2. However, the low conductivity of POMs restricts the maximum current density to less than 20 mA cm^{-2}. Thus, further research is required to develop POMs that can operate at higher current densities. Additionally, the mechanistic understanding of POM-based catalysis is still in its early stages, lacking theoretical frameworks to guide the enhancement of these catalysts.

Compared to heterostructures, constructing chemical bonds between active components and acid-resistant substrates is a more effective strategy to mitigate corrosion. Gao *et al.*[20] developed a semi-rigid single-metal-site catalyst anchored on a Th-MOF, which featured open metal sites and rotatable anionic sites, providing greater flexibility for reaction intermediates. The $CoCl_2$@Th-MOF catalyst showed an overpotential of 388 mV to reach 10 mA cm^{-2} in 0.1 M $HClO_4$ electrolyte.

6. Conclusion and perspectives

In recent years, significant efforts have been directed toward the development of low-cost OER catalysts in acids with well-balanced activity and stability. This review summarizes recent key advances in this field, including the mechanistic insights, *in situ*/*operando* techniques, and synthetic/modification strategies for non-noble metal OER catalysts under acidic conditions. By discussing the conventional mechanisms such as the AEM and LOM, alongside newly proposed ones such as the OPM and PDAM, the mechanistic framework for acidic OER has been enriched.

Unlike alkaline OER, acidic OER catalysts must withstand high potentials and low pH environments, which poses unique stability challenges. High-throughput screening methods

© 2025 The Author(s). Published by the Royal Society of Chemistry

Open Access Article. Published on 05 February 2025. Downloaded on 2/13/2026 4:26:31 AM.
This article is licensed under a Creative Commons Attribution-NonCommercial 3.0 Unported Licence.

combined with Pourbaix diagrams offer a promising alternative to conventional experimental approaches for identifying stable catalyst compositions. Also, advanced *in situ*/*operando* techniques that monitor surface evolution and intermediate species during reactions are crucial for elucidating detailed mechanisms. Despite these efforts, most acidic OER catalysts remain at the laboratory testing stage due to insufficient stability, which is far from meeting the requirements for practical application (Fig. 7). In addition, the lack of standardized evaluation methods hinders the precise evaluation of the intrinsic activity of catalysts. Finally, testing OER catalysts in a membrane electrode assembly (MEA) setup would be critical to evaluate the catalytic performance under practical working conditions. The following sections provide perspectives on overcoming these challenges for non-noble metal acidic OER catalysts.

6.1 Breaking the activity–stability tradeoff

Stability is a critical challenge for non-noble metal catalysts under acidic conditions, and prioritizing activity at the expense of stability is not a sustainable strategy (Fig. 8). The stability issues mainly come from the inherent instability of the lattice structure in acidic solutions and at high potentials. Modification strategies such as element doping, surface coating and phase engineering have shown promise in addressing these limitations. Mechanistic studies indicate that OER processes often involve multiple pathways simultaneously. Enhancing the contributions of the AEM, OPM, and PDAM pathways while minimizing the lattice oxygen involvement might significantly improve acid stability.

Besides intrinsic stability, external factors also play a critical role in catalyst durability. These include detachment of catalyst active sites caused by bubble generation at high current density, peeling of catalysts from the current collector due to week binder adhesion, and corrosion of the carbon current collector at high potentials. Addressing these issues requires innovative structural design, such as hydrophilic/hydrophobic interfaces to facilitate bubble removal, binder-free self-supported catalysts, and high-strength binders to improve catalyst adhesion.

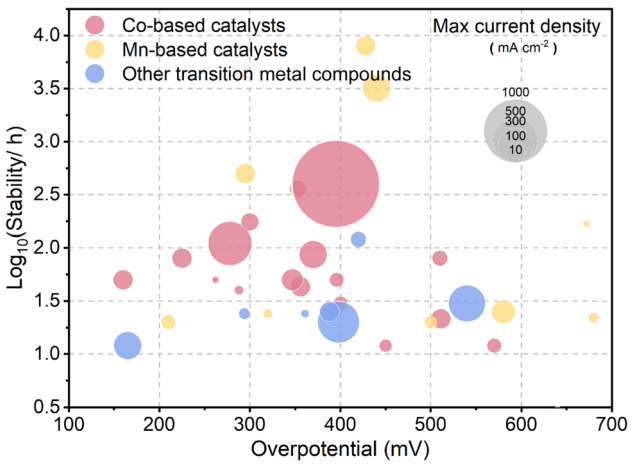

Fig. 8 Benchmarking of noble-metal-free OER electrocatalysts tested in acidic media. Overpotentials and stability of the catalysts at a current density of 10 mA cm^{-2}. See detailed information in Table 1 for noble-metal-free catalysts.

6.2 Establishing unified catalyst evaluation criteria

The lack of standardized evaluation methods for acidic OER catalysts complicates the comparison of performance across studies. Differences in preparation methods, characterization techniques, and testing parameters can significantly affect key performance metrics, such as the onset potential and operational stability (Table 1). For powder catalysts, a mixed slurry of catalyst and binder is generally sprayed on carbon/titanium substrates or drop cast on glassy carbon electrodes to evaluate their performance. The measurements of onset potential and catalytic activity often ignore the impact of mass loading or true catalyst surface area. Mass activity or electrochemical active surface area (ECSA) normalization should be incorporated to better reflect intrinsic activity of catalysts.

Performance assessments, typically conducted in a H-cell or single chamber three-electrode system, do not fully reflect the real-world scenario under PEMWE conditions. Firstly, liquid electrochemical cells and MEA-based solid electrolyzers exhibit a distinct catalyst–electrolyte interface structure. Interfacial chemical environments have been known to profoundly affect the electrocatalytic reactions. Secondly, mass transport processes are different in liquid cells and solid electrolyzers. A properly designed MEA would favor the supply of water to the catalyst layer and ensure rapid release of oxygen gas at the anode, which supports water electrolysis at A cm^{-2}-level high current density. Thirdly, degradation mechanisms might be different. For example, in liquid electrochemical cells, violent gas release at high current density might lead to detachment of catalysts from the current collector. While in solid electrolyzers, dissolution of metal ions from catalysts might cause more severe activity degradation. These differences result in notable performance discrepancies when evaluating the same catalysts in a three-electrode liquid cell and PEMWE (Fig. 9). Additionally, incorporating a reference electrode ensures the precise measurement of the overpotential of an individual electrode, which is a conventional practice in liquid electrochemical cells but technically challenging in MEA-type electrolyzers. Finally, evaluations in PEMWE systems are essential but remain underreported due to the challenges associated with the assembly of these systems. Addressing this gap is crucial to bridge the disparity between laboratory-scale testing and practical applications.

6.3 Overcoming application challenges in PEM water electrolysis

PEMWE systems face unique challenges compared with conventional open electrolysis systems due to their distinct device structures, assembly procedures, proton conduction mechanisms, and gas transmission processes. Key challenges in PEMWE systems are typically associated with electrolyte conditions, catalyst-collector bonding stability, membrane–electrolyte–catalyst interface interactions, and metal cation toxicity to proton membranes.

© 2025 The Author(s). Published by the Royal Society of Chemistry

Open Access Article. Published on 05 February 2025. Downloaded on 2/13/2026 4:26:31 AM.
This article is licensed under a Creative Commons Attribution-NonCommercial 3.0 Unported Licence.

Table 1 Catalytic performances of non-noble-metal catalysts for the OER under acidic conditions

Catalyst	Morphology	Electrolyte	Support	Loading (mg cm^{-2})	Overpotential @ 10 mA cm^{-2} (mV)	Stability	Max current d ensity (mA)
40-Co_3O_4@C/GPO[75]	Nanoparticles	1 M H_2SO_4	Pocket working electrode	20	356	43 h @ 10 mA cm^{-2}	100
Co_3O_4 [117]	Film	0.5 M H_2SO_4	FTO	0.182	570	12 h @ 10 mA cm^{-2}	50
Ag–Co_3O_4 [66]	Nanosheets	0.5 M H_2SO_4	Glassy carbon electrode	0.2	470	—	60
$Co_{3-x}Ba_xO_4$ [14]	Nanosheets	0.5 M H_2SO_4	Carbon paper	1.6	278	110 h @ 10 mA cm^{-2}	500
Fe–Co_3O_4@C[60]	Nanoparticles	0.5 M H_2SO_4	FTO	1.1	396	50 h @ 10 mA cm^{-2}	50
LaMnCo-fiber[42]	Fiber	0.1 M $HClO_4$	RDE	0.26	353	360 h @ 10 mA cm^{-2}	70
3D Co_3O_4/NC-250 [62]	Nanoarrays/cubes	0.5 M H_2SO_4	Carbon paper	0.5	225	80 h @ 10 mA cm^{-2}	100
P–Co_3O_4 [65]	Nanowires	0.1 M $HClO_4$	RDE	0.07	400	30 h @ 10 mA cm^{-2}	50
CeO_2/Co–Ni–P–O_x [47]	Nanorods	0.5 M H_2SO_4	Carbon paper	0.6	262	50 h @ 5 mA cm^{-2}	10
Co_3O_4/CeO_2 [52]	Nanosheets	0.5 M H_2SO_4	Carbon paper	—	347	50 h @ 10 mA cm^{-2}	120
TRGO@ZnO/Co_3O_4 [70]	Nanoparticles	0.5 M H_2SO_4	Carbon paper	0.01	160	50 h @ 10 mA cm^{-2}	100
PdO@Co_3O_4 [69]	Nanorods/nanospheres	0.1 M HNO_3	RDE	1.36	523	2 h @ 10 mA cm^{-2}	50
Co/29BC[73]	Nanoparticles	0.5 M H_2SO_4	Carbon paper	—	450	12 h @ 10 mA cm^{-2}	40
TiO_2/Co_3O_4 [67]	Nanorods	0.5 M H_2SO_4	Pt/Ti	—	510	80 h @ 10 mA cm^{-2}	60
Co_3O_4@C[74]	Nanosheets	0.5 M H_2SO_4	Carbon paper	5	370	86.8 h @ 100 mA cm^{-2}	200
FTO@Co_3O_4 [76]	Nanoparticles	0.5 M H_2SO_4	Carbon paper	3	511	21.5 h @ 10 mA cm^{-2}	100
Co_2MnO_4 [63]	Film	pH = 1H_2SO_4	FTO	10	395	400 h @ 200 mA cm^{-2}	2000
$Co_2Sb_2O_7$ [82]	Bulk	0.5 M H_2SO_4	Glassy carbon electrode	0.28	288	40 h @ 1 mA cm^{-2}	20
Co_2TiO_4 [78]	Nanoparticles	0.5 M H_2SO_4	Carbon paper	—	513	—	60
γ-MnO_2 [88]	Film	1 M H_2SO_4	Carbon paper	3.5	428	8000 h at 10 mA cm^{-2}	100
M94% [87]	Nanoarrays	1 M H_2SO_4	Pt/Ti mesh	7.2 (Mn loading)	440	3200 h at 200 mA cm^{-2}	200
R20-Mn[118]	Nanoplates	0.5 M H_2SO_4	Carbon paper	1	210	20 h at 10 mA cm^{-2}	50
$MnFeF_{4.6}O_{0.2}$ [95]	Amorphous	0.5 M H_2SO_4	Carbon paper	1	500	20 h @ 10 mA cm^{-2}	40
$Mn_{7.5}O_{10}Br_3$ [89]	Film	0.5 M H_2SO_4	Carbon paper	7.2	295	500 h @ 10 mA cm^{-2}	100
Si–MnO_2 [99]	Film	0.1 M H_2SO_4	FTO	—	640	~3 h @ 10 mA cm^{-2}	15
Pb/Pb–MnO_2 [98]	Film	1.63 M H_2SO_4	Lead substrate	—	655 (50 mA cm^{-2})	—	150
$MnxSb_{1-x}O_z$ [102]	Film	1 M H_2SO_4	Pt/Ti/SiO_2/ Si substrates	(Sb + Mn loading) 20.47 nmol mm^{-2}	580	25 h @1 mA cm^{-2}	140
$Cu_{1.5}Mn_{1.5}O_4$:10F[94]	Nanoparticles	0.5 M H_2SO_4	Porous Ti	1	320 (9.15 mA cm^{-2})	24 h @ 16 mA cm^{-2}	20
$Ni_{0.5}Mn_{0.5}Sb_{1.7}O_y$ [100]	Film	1 M H_2SO_4	ATO	(Ni + Sb + Mn loading) 13 μmol cm^{-2}	672	168 h @ 10 mA cm^{-2}	10
$(Mn_{0.8}Nb_{0.2})O_2$:10F[93]	Nanorods	0.5 M H_2SO_4	Titanium foils	0.3	680	22 h @ 1.9 V (*vs.* RHE)	25
1T MoS_2 [105]	Nanosheets	0.5 M H_2SO_4	Carbon paper	1	420	120 h @ 10 mA cm^{-2}	60
P-NSC/$Ni_4Fe_5S_8$-1000 [106]	Nanoparticles	0.5 M H_2SO_4	Glassy carbon electrode	0.4	300 (1 mA cm^{-2})	—	15
MoS_2/Co_9S_8/Ni_3S_2/Ni[17]	Nanorods/nanosheets	0.5 M H_2SO_4	Ni foam	1.86	255	1.3 h @ 1.53 V (*vs.* RHE)	100
NiFeP[16]	Amorphous	0.05 M H_2SO_4	Self-standing	—	540	30 h @ 10 mA cm^{-2}	350
CoMnP/Ni_2P[107]	Nanosheets/ microplate arrays	0.5 M H_2SO_4	Ni foam	1.68	165	12 h @ 10 mA cm^{-2}	200

© 2025 The Author(s). Published by the Royal Society of Chemistry

Open Access Article. Published on 05 February 2025. Downloaded on 2/13/2026 4:26:31 AM.
This article is licensed under a Creative Commons Attribution-NonCommercial 3.0 Unported Licence.

Table 1 (*Contd.*)

Catalyst	Morphology	Electrolyte	Support	Loading (mg cm^{-2})	Overpotential @ 10 mA cm^{-2} (mV)	Stability	Max current density (mA)
TiN@$Co_{5.47}N$[15]	Film	0.1 M $HClO_4$	Ti mesh	—	398 (50 mA cm^{-2})	20 h @ 100 mA cm^{-2}	450
FeN_4/NF/EG[103]	Nanofibers	0.5 M H_2SO_4	Exfoliated graphene	5.7	294	24 h @ 20 mA cm^{-2}	30
Mn-doped FeP/$Co_3(PO_4)_2$[111]	Nanosheets	0.5 M H_2SO_4	Carbon paper	1.2	390	—	50
CWO-del-48[112]	Delaminated nanoparticles	0.5 M H_2SO_4	Carbon paper	1.4	300	175 h @ 10 mA cm^{-2}	80
$CoCl_2$@Th-BPYDC[20]	Nanoparticles	0.1 M $HClO_4$	Carbon paper	0.075	388	25 h @ 1.68 V (*vs.* RHE)	100
Ba[Co-POM][18]	Nanoparticles	1 M H_2SO_4	Carbon paper	(Ba + Co loading) 16.13 μmol cm^{-2}	361	24 h @ 1.48 V (*vs.* RHE)	15

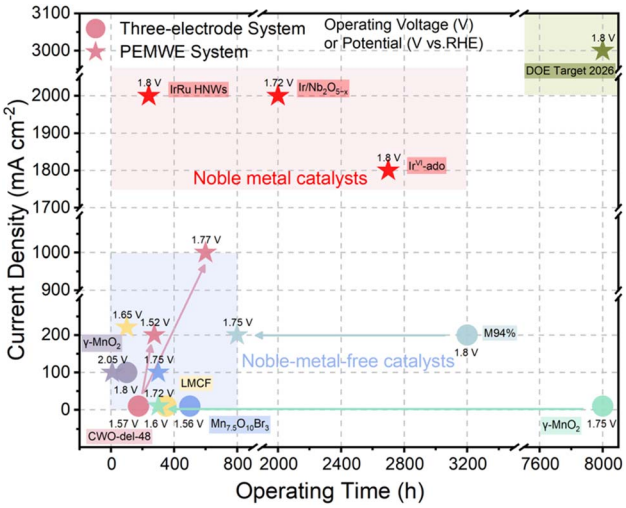

Fig. 9 PEMWE and three-electrode electrochemical cell performance comparison of reported non-noble metal OER catalysts. Representative Ir-based catalysts and DOE target 2026 are given for comparison.

Firstly, pure water is supplied to PEMWEs rather than acidic electrolyte, which requires a higher overpotential. Secondly, titanium-based substrates, such as titanium felt or mesh, are commonly used but suffer from passivation due to the formation of titanium oxide layers, hampering interfacial electron transfer. Free-standing catalysts typically require pre-treatments of titanium substrates with hazardous chemicals (*e.g.*, hydrofluoric acid, nitric acid, and oxalic acid) and/or at high temperatures, which remains a significant hurdle. Alternative surface modification approaches, such as platinum or gold plating and nitridation with plasma, have shown promise in improving interfacial stability. Thirdly, the interaction between catalysts and PEMs remains poorly understood. Real-time monitoring of these inorganic–organic interfaces under operating conditions is critical for understanding their behavior and optimizing device performance.[128,129]

Overall, PEMWE systems with multiple interfaces and a complex operational environment face greater challenges compared to conventional three-electrode systems. Deeper exploration of these interfaces and their interactions is essential to clarify the connection between fundamental mechanisms and practical applications. By addressing these challenges, future research can enable the rational design of non-noble metal acidic OER catalysts with improved performance and scalability, paving the way for their widespread adoption in renewable energy technologies.

Data availability

The data that support the findings of this study are available from the corresponding author, H. B. Wu, upon reasonable request.

Author contributions

Junwei Han: conceptualization, methodology, writing – original draft, visualization; Qian Liu: writing – review & editing,

© 2025 The Author(s). Published by the Royal Society of Chemistry

Open Access Article. Published on 05 February 2025. Downloaded on 2/13/2026 4:26:31 AM. This article is licensed under a Creative Commons Attribution-NonCommercial 3.0 Unported Licence.

visualization; Yue Yang: writing – review & editing; Hao Bin Wu: investigation, funding acquisition, writing – review & editing, validation, supervision.

Conflicts of interest

There are no conflicts to declare.

Acknowledgements

H. B. W. acknowledges the funding support from the National Key R&D Program of China (2023YFB4203900) and the Fundamental Research Funds for the Central Universities (226-2024-00075).

References

1 S. Chu and A. Majumdar, Opportunities and challenges for a sustainable energy future, *Nature*, 2012, **488**, 294–303.
2 I. Staffell, D. Scamman, A. Velazquez Abad, P. Balcombe, P. E. Dodds, P. Ekins, N. Shah and K. R. Ward, The role of hydrogen and fuel cells in the global energy system, *Energy Environ. Sci.*, 2019, **12**, 463–491.
3 S. Aslam, S. Rani, K. Lal, M. Fatima, T. Hardwick, B. Shirinfar and N. Ahmed, Electrochemical hydrogen production: sustainable hydrogen economy, *Green Chem.*, 2023, **25**, 9543–9573.
4 T. Ioroi, Z. Siroma, S. I. Yamazaki and K. Yasuda, Electrocatalysts for PEM Fuel Cells, *Adv. Energy Mater.*, 2018, **9**, 1801284.
5 M. Carmo, D. L. Fritz, J. Mergel and D. Stolten, A comprehensive review on PEM water electrolysis, *Int. J. Hydrogen Energy*, 2013, **38**, 4901–4934.
6 H. Y. Lin, Z. X. Lou, Y. Ding, X. Li, F. Mao, H. Y. Yuan, P. F. Liu and H. G. Yang, Oxygen Evolution Electrocatalysts for the Proton Exchange Membrane Electrolyzer: Challenges on Stability, *Small Methods*, 2022, **6**, e2201130.
7 A. Minguzzi, O. Lugaresi, E. Achilli, C. Locatelli, A. Vertova, P. Ghigna and S. Rondinini, Observing the oxidation state turnover in heterogeneous iridium-based water oxidation catalysts, *Chem. Sci.*, 2014, **5**, 3591–3597.
8 H. Zhu, Y. Wang, Z. Jiang, B. Deng, Y. Xin and Z. J. Jiang, Defect Engineering Promoted Ultrafine Ir Nanoparticle Growth and Sr Single-Atom Adsorption on TiO_2 Nanowires to Achieve High-Performance Overall Water Splitting in Acidic Media, *Adv. Energy Mater.*, 2024, **14**, 2303987.
9 J. He, X. Zhou, P. Xu and J. Sun, Regulating Electron Redistribution of Intermetallic Iridium Oxide by Incorporating Ru for Efficient Acidic Water Oxidation, *Adv. Energy Mater.*, 2021, **11**, 2102883.
10 H. Jin, S. Choi, G. J. Bang, T. Kwon, H. S. Kim, S. J. Lee, Y. Hong, D. W. Lee, H. S. Park, H. Baik, Y. Jung, S. J. Yoo and K. Lee, Safeguarding the RuO_2 phase against lattice oxygen oxidation during acidic water electrooxidation, *Energy Environ. Sci.*, 2022, **15**, 1119–1130.
11 N. Yao, H. Jia, J. Zhu, Z. Shi, H. Cong, J. Ge and W. Luo, Atomically dispersed Ru oxide catalyst with lattice oxygen participation for efficient acidic water oxidation, *Chem*, 2023, **9**, 1882–1896.
12 Z. Chen, X. Duan, W. Wei, S. Wang and B.-J. Ni, Electrocatalysts for acidic oxygen evolution reaction: Achievements and perspectives, *Nano Energy*, 2020, **78**, 105392.
13 C. Wang, R. Deng, M. Guo and Q. Zhang, Recent progress of advanced Co_3O_4-based materials for electrocatalytic oxygen evolution reaction in acid: from rational screening to efficient design, *Int. J. Hydrogen Energy*, 2023, **48**, 31920–31942.
14 N. Wang, P. Ou, R. K. Miao, Y. Chang, Z. Wang, S.-F. Hung, J. Abed, A. Ozden, H.-Y. Chen, H.-L. Wu, J. E. Huang, D. Zhou, W. Ni, L. Fan, Y. Yan, T. Peng, D. Sinton, Y. Liu, H. Liang and E. H. Sargent, Doping Shortens the Metal/Metal Distance and Promotes OH Coverage in Non-Noble Acidic Oxygen Evolution Reaction Catalysts, *J. Am. Chem. Soc.*, 2023, **145**, 7829–7836.
15 D. Guo, Z. Wan, Y. Li, B. Xi and C. Wang, TiN @ $Co_{5.47}N$ Composite Material Constructed by Atomic Layer Deposition as Reliable Electrocatalyst for Oxygen Evolution Reaction, *Adv. Funct. Mater.*, 2020, **31**, 2008511.
16 F. Hu, S. Zhu, S. Chen, Y. Li, L. Ma, T. Wu, Y. Zhang, C. Wang, C. Liu, X. Yang, L. Song, X. Yang and Y. Xiong, Amorphous Metallic NiFeP: A Conductive Bulk Material Achieving High Activity for Oxygen Evolution Reaction in Both Alkaline and Acidic Media, *Adv. Mater.*, 2017, **29**, 1606570.
17 Y. Yang, H. Yao, Z. Yu, S. M. Islam, H. He, M. Yuan, Y. Yue, K. Xu, W. Hao, G. Sun, H. Li, S. Ma, P. Zapol and M. G. Kanatzidis, Hierarchical Nanoassembly of MoS_2/Co_9S_8/Ni_3S_2/Ni as a Highly Efficient Electrocatalyst for Overall Water Splitting in a Wide pH Range, *J. Am. Chem. Soc.*, 2019, **141**, 10417–10430.
18 M. Blasco-Ahicart, J. Soriano-López, J. J. Carbó, J. M. Poblet and J. R. Galan-Mascaros, Polyoxometalate electrocatalysts based on earth-abundant metals for efficient water oxidation in acidic media, *Nat. Chem.*, 2017, **10**, 24–30.
19 J. Qi, Y. P. Lin, D. Chen, T. Zhou, W. Zhang and R. Cao, Autologous Cobalt Phosphates with Modulated Coordination Sites for Electrocatalytic Water Oxidation, *Angew. Chem., Int. Ed.*, 2020, **59**, 8917–8921.
20 Z. Gao, Y. Lai, L. Gong, L. Zhang, S. Xi, J. Sun, L. Zhang and F. Luo, Robust Th-MOF-Supported Semirigid Single-Metal-Site Catalyst for an Efficient Acidic Oxygen Evolution Reaction, *ACS Catal.*, 2022, **12**, 9101–9113.
21 R. Y. Fan, Y. S. Zhang, J. Y. Lv, G. Q. Han, Y. M. Chai and B. Dong, The Promising Seesaw Relationship Between Activity and Stability of Ru-Based Electrocatalysts for Acid Oxygen Evolution and Proton Exchange Membrane Water Electrolysis, *Small*, 2023, **20**, 2304636.
22 T. Nishimoto, T. Shinagawa, T. Naito and K. Takanabe, Microkinetic assessment of electrocatalytic oxygen evolution reaction over iridium oxide in unbuffered conditions, *J. Catal.*, 2020, **391**, 435–445.

© 2025 The Author(s). Published by the Royal Society of Chemistry

Open Access Article. Published on 05 February 2025. Downloaded on 2/13/2026 4:26:31 AM. This article is licensed under a Creative Commons Attribution-NonCommercial 3.0 Unported Licence.

23 Z. Wang, Y.-R. Zheng, I. Chorkendorff and J. K. Nørskov, Acid-Stable Oxides for Oxygen Electrocatalysis, *ACS Energy Lett.*, 2020, **5**, 2905–2908.
24 G. Mirshekari, R. Ouimet, Z. Zeng, H. Yu, S. Bliznakov, L. Bonville, A. Niedzwiecki, C. Capuano, K. Ayers and R. Maric, High-performance and cost-effective membrane electrode assemblies for advanced proton exchange membrane water electrolyzers: Long-term durability assessment, *Int. J. Hydrogen Energy*, 2021, **46**, 1526–1539.
25 X. Li, Y. Yao, Y. Tian, J. Jia, W. Ma, X. Yan and J. Liang, Recent advances in key components of proton exchange membrane water electrolysers, *Mater. Chem. Front.*, 2024, **8**, 2493–2510.
26 T. Zhang, L. Meng, C. Chen, L. Du, N. Wang, L. Xing, C. Tang, J. Hu and S. Ye, Similarities and Differences between Gas Diffusion Layers Used in Proton Exchange Membrane Fuel Cell and Water Electrolysis for Material and Mass Transport, *Adv. Sci.*, 2024, **11**, e2309440.
27 R. T. Liu, Z. L. Xu, F. M. Li, F. Y. Chen, J. Y. Yu, Y. Yan, Y. Chen and B. Y. Xia, Recent advances in proton exchange membrane water electrolysis, *Chem. Soc. Rev.*, 2023, **52**, 5652–5683.
28 C. Biaku, N. Dale, M. Mann, H. Salehfar, A. Peters and T. Han, A semiempirical study of the temperature dependence of the anode charge transfer coefficient of a 6kW PEM electrolyzer, *Int. J. Hydrogen Energy*, 2008, **33**, 4247–4254.
29 B. Mohamed, B. Alli and B. Ahmed, Using the hydrogen for sustainable energy storage: Designs, modeling, identification and simulation membrane behavior in PEM system electrolyser, *J. Energy Storage*, 2016, **7**, 270–285.
30 K. Ayers, High efficiency PEM water electrolysis: enabled by advanced catalysts, membranes, and processes, *Curr. Opin. Chem. Eng.*, 2021, **33**, 100719.
31 A. Makhsoos, M. Kandidayeni, B. G. Pollet and L. Boulon, A perspective on increasing the efficiency of proton exchange membrane water electrolyzers– a review, *Int. J. Hydrogen Energy*, 2023, **48**, 15341–15370.
32 K. Ayers, The potential of proton exchange membrane–based electrolysis technology, *Curr. Opin. Electrochem.*, 2019, **18**, 9–15.
33 J. Rossmeisl, A. Logadottir and J. K. Nørskov, Electrolysis of water on (oxidized) metal surfaces, *Chem. Phys.*, 2005, **319**, 178–184.
34 V. Stamenkovic, B. S. Mun, K. J. J. Mayrhofer, P. N. Ross, N. M. Markovic, J. Rossmeisl, J. Greeley and J. K. Nørskov, Changing the Activity of Electrocatalysts for Oxygen Reduction by Tuning the Surface Electronic Structure, *Angew. Chem., Int. Ed.*, 2006, **45**, 2897–2901.
35 F. Studt, F. Abild-Pedersen, H. A. Hansen, I. C. Man, J. Rossmeisl and T. Bligaard, Volcano Relation for the Deacon Process over Transition-Metal Oxides, *ChemCatChem*, 2010, **2**, 98–102.
36 K. L. Svane and J. Rossmeisl, Theoretical Optimization of Compositions of High-Entropy Oxides for the Oxygen Evolution Reaction, *Angew. Chem., Int. Ed.*, 2022, **134**, e202201146.
37 I. C. Man, H. Y. Su, F. Calle-Vallejo, H. A. Hansen, J. I. Martínez, N. G. Inoglu, J. Kitchin, T. F. Jaramillo, J. K. Nørskov and J. Rossmeisl, Universality in Oxygen Evolution Electrocatalysis on Oxide Surfaces, *ChemCatChem*, 2011, **3**, 1159–1165.
38 R. Zhang, L. Pan, B. Guo, Z.-F. Huang, Z. Chen, L. Wang, X. Zhang, Z. Guo, W. Xu, K. P. Loh and J.-J. Zou, Tracking the Role of Defect Types in Co_3O_4 Structural Evolution and Active Motifs during Oxygen Evolution Reaction, *J. Am. Chem. Soc.*, 2023, **145**, 2271–2281.
39 H. M. A. Amin and H. Baltruschat, How many surface atoms in Co_3O_4 take part in oxygen evolution? Isotope labeling together with differential electrochemical mass spectrometry, *Phys. Chem. Chem. Phys.*, 2017, **19**, 25527–25536.
40 H. M. A. Amin, P. Königshoven, M. Hegemann and H. Baltruschat, Role of Lattice Oxygen in the Oxygen Evolution Reaction on Co_3O_4: Isotope Exchange Determined Using a Small-Volume Differential Electrochemical Mass Spectrometry Cell Design, *Anal. Chem.*, 2019, **91**, 12653–12660.
41 A. Grimaud, W. T. Hong, Y. Shao-Horn and J. M. Tarascon, Anionic redox processes for electrochemical devices, *Nat. Mater.*, 2016, **15**, 121–126.
42 L. Lin, Q. Fu, R. Wang, T. Yao, X. Wang and B. Song, Spinel-Type Oxides for Acidic Oxygen Evolution Reaction: Mechanism, Modulation, and Perspective, *Adv. Energy Sustainability Res.*, 2023, **4**, 2300075.
43 X. Rong, J. Parolin and A. M. Kolpak, A Fundamental Relationship between Reaction Mechanism and Stability in Metal Oxide Catalysts for Oxygen Evolution, *ACS Catal.*, 2016, **6**, 1153–1158.
44 Q. Liang, G. Brocks and A. Bieberle-Hütter, Oxygen evolution reaction (OER) mechanism under alkaline and acidic conditions, *J. Phys.: Energy*, 2021, **3**, 026001.
45 I. Barlocco, L. A. Cipriano, G. Di Liberto and G. Pacchioni, Does the Oxygen Evolution Reaction follow the classical OH*, O*, OOH* path on single atom catalysts?, *J. Catal.*, 2023, **417**, 351–359.
46 Y. Hao, S.-F. Hung, W.-J. Zeng, Y. Wang, C. Zhang, C.-H. Kuo, L. Wang, S. Zhao, Y. Zhang, H.-Y. Chen and S. Peng, Switching the Oxygen Evolution Mechanism on Atomically Dispersed Ru for Enhanced Acidic Reaction Kinetics, *J. Am. Chem. Soc.*, 2023, **145**, 23659–23669.
47 A. M. Patel, J. K. Nørskov, K. A. Persson and J. H. Montoya, Efficient Pourbaix diagrams of many-element compounds, *Phys. Chem. Chem. Phys.*, 2019, **21**, 25323–25327.
48 A. Minguzzi, F.-R. F. Fan, A. Vertova, S. Rondinini and A. J. Bard, Dynamic potential-pH diagrams application to electrocatalysts for wateroxidation, *Chem. Sci.*, 2012, **3**, 217–229.
49 S. Cherevko, Stabilization of non-noble metal electrocatalysts for acidic oxygen evolution reaction, *Curr. Opin. Electrochem.*, 2023, **38**, 101213.
50 M. Bajdich, M. García-Mota, A. Vojvodic, J. K. Nørskov and A. T. Bell, Theoretical Investigation of the Activity of Cobalt

Open Access Article. Published on 05 February 2025. Downloaded on 2/13/2026 4:26:31 AM. This article is licensed under a Creative Commons Attribution-NonCommercial 3.0 Unported Licence.

Oxides for the Electrochemical Oxidation of Water, *J. Am. Chem. Soc.*, 2013, **135**, 13521–13530.

51 L. Chong, G. Gao, J. Wen, H. Li, H. Xu, Z. Green, J. D. Sugar, A. J. Kropf, W. Xu, X.-M. Lin, H. Xu, L.-W. Wang and D.-J. Liu, La- and Mn-doped cobalt spinel oxygen evolution catalyst for proton exchange membrane electrolysis, *Science*, 2023, **380**, 609–616.

52 B.-R. Chen, W. Sun, D. A. Kitchaev, K. H. Stone, R. C. Davis, G. Ceder, L. T. Schelhas and M. F. Toney, Kinetic origins of the metastable zone width in the manganese oxide Pourbaix diagram, *J. Mater. Chem. A*, 2021, **9**, 7857–7867.

53 Y. Shi, H. Wu, J. Chang, Z. Tang and S. Lu, Progress on the mechanisms of Ru-based electrocatalysts for the oxygen evolution reaction in acidic media, *J. Energy Chem.*, 2023, **85**, 220–238.

54 Z. Shi, X. Wang, J. Ge, C. Liu and W. Xing, Fundamental understanding of the acidic oxygen evolution reaction: mechanism study and state-of-the-art catalysts, *Nanoscale*, 2020, **12**, 13249–13275.

55 Y.-H. Wang, S. Zheng, W.-M. Yang, R.-Y. Zhou, Q.-F. He, P. Radjenovic, J.-C. Dong, S. Li, J. Zheng, Z.-L. Yang, G. Attard, F. Pan, Z.-Q. Tian and J.-F. Li, In situ Raman spectroscopy reveals the structure and dissociation of interfacial water, *Nature*, 2021, **600**, 81–85.

56 J. Liu, T. Wang, X. Liu, H. Shi, S. Li, L. Xie, Z. Cai, J. Han, Y. Huang, G. Wang and Q. Li, Reducible Co^{3+}-O Sites of Co-Ni-P-O_x on CeO_2 Nanorods Boost Acidic Water Oxidation via Interfacial Charge Transfer-Promoted Surface Reconstruction, *ACS Catal.*, 2023, **13**, 5194–5204.

57 Z. Chen, Q. Fan, J. Zhou, X. Wang, M. Huang, H. Jiang and H. Cölfen, Toward Understanding the Formation Mechanism and OER Catalytic Mechanism of Hydroxides by *In Situ* and Operando Techniques, *Angew. Chem., Int. Ed.*, 2023, **62**, 101213.

58 P. M. Radjenovic, R.-Y. Zhou, J.-C. Dong and J.-F. Li, Watching Reactions at Solid-Liquid Interfaces with *in Situ* Raman Spectroscopy, *J. Phys. Chem. C*, 2021, **125**, 26285–26295.

59 M. Chen, D. Liu, L. Qiao, P. Zhou, J. Feng, K. W. Ng, Q. Liu, S. Wang and H. Pan, In-situ/operando Raman techniques for in-depth understanding on electrocatalysis, *Chem. Eng. J.*, 2023, **461**, 141939.

60 K. Natarajan, E. Munirathinam and T. C. K. Yang, Operando Investigation of Structural and Chemical Origin of Co_3O_4 Stability in Acid under Oxygen Evolution Reaction, *ACS Appl. Mater. Interfaces*, 2021, **13**, 27140–27148.

61 J. Huang, H. Sheng, R. D. Ross, J. Han, X. Wang, B. Song and S. Jin, Modifying redox properties and local bonding of Co_3O_4 by CeO_2 enhances oxygen evolution catalysis in acid, *Nat. Commun.*, 2021, **12**, 3036.

62 J. Wang, H. Kim, H. Lee, Y.-J. Ko, M. H. Han, W. Kim, J. M. Baik, J.-Y. Choi, H.-S. Oh and W. H. Lee, Sb incorporated into oxides enhances stability in acid during the oxygen evolution reaction by inhibiting structural distortion, *Nano Energy*, 2023, **110**, 108355.

63 X. Zhang, C. Feng, B. Dong, C. Liu and Y. Chai, High-Voltage-Enabled Stable Cobalt Species Deposition on MnO_2 for Water Oxidation in Acid, *Adv. Mater.*, 2023, **35**, 2207066.

64 S. Schlucker, Surface-enhanced Raman spectroscopy: concepts and chemical applications, *Angew Chem. Int. Ed. Engl.*, 2014, **53**, 4756–4795.

65 L. Fang, S. Seifert, R. E. Winans and T. Li, Understanding Synthesis and Structural Variation of Nanomaterials Through In Situ/Operando XAS and SAXS, *Small*, 2022, **18**, e2106017.

66 A. M. Ullman, C. N. Brodsky, N. Li, S. L. Zheng and D. G. Nocera, Probing Edge Site Reactivity of Oxidic Cobalt Water Oxidation Catalysts, *J. Am. Chem. Soc.*, 2016, **138**, 4229–4236.

67 F. Zeng, C. Mebrahtu, L. Liao, A. K. Beine and R. Palkovits, Stability and deactivation of OER electrocatalysts: A review, *J. Energy Chem.*, 2022, **69**, 301–329.

68 S. R. Ede and Z. Luo, Tuning the intrinsic catalytic activities of oxygen-evolution catalysts by doping: a comprehensive review, *J. Mater. Chem. A*, 2021, **9**, 20131–20163.

69 D. Senthil Raja, P.-Y. Cheng, C.-C. Cheng, S.-Q. Chang, C.-L. Huang and S.-Y. Lu, In-situ grown metal-organic framework-derived carbon-coated Fe-doped cobalt oxide nanocomposite on fluorine-doped tin oxide glass for acidic oxygen evolution reaction, *Appl. Catal., B*, 2022, **303**, 120899.

70 E. O. Nwanebu and S. Omanovic, The influence of Ni_xCo_{1-x}-oxide composition on its electrocatalytic activity in the oxygen evolution reaction, *Mater. Chem. Phys.*, 2019, **228**, 80–88.

71 A. Li, S. Kong, C. Guo, H. Ooka, K. Adachi, D. Hashizume, Q. Jiang, H. Han, J. Xiao and R. Nakamura, Enhancing the stability of cobalt spinel oxide towards sustainable oxygen evolution in acid, *Nat. Catal.*, 2022, **5**, 109–118.

72 I. Abidat, N. Bouchenafa-Saib, A. Habrioux, C. Comminges, C. Canaff, J. Rousseau, T. W. Napporn, D. Dambournet, O. Borkiewicz and K. B. Kokoh, Electrochemically induced surface modifications of mesoporous spinels ($Co_3O_{4-\delta}$, $MnCo_2O_{4-\delta}$, $NiCo_2O_{4-\delta}$) as the origin of the OER activity and stability in alkaline medium, *J. Mater. Chem. A*, 2015, **3**, 17433–17444.

73 X. Yang, J. Cheng, H. Li, Y. Xu, W. Tu and J. Zhou, Self-supported N-doped hierarchical Co_3O_4 electrocatalyst with abundant oxygen vacancies for acidic water oxidation, *Chem. Eng. J.*, 2023, **465**, 142745.

74 F. Shang, H. He, P. Li, H. Cai, B. An, X. Li, S. Yang, Z. Sun and B. Wang, PO6 geometric configuration unit enhanced electrocatalytic performance of Co_3O_4 in acidic oxygen evolution, *J. Colloid Interface Sci.*, 2023, **641**, 329–337.

75 K.-L. Yan, J.-F. Qin, J.-H. Lin, B. Dong, J.-Q. Chi, Z.-Z. Liu, F.-N. Dai, Y.-M. Chai and C.-G. Liu, Probing the active sites of Co_3O_4 for the acidic oxygen evolution reaction by modulating the Co^{2+}/Co^{3+} ratio, *J. Mater. Chem. A*, 2018, **6**, 5678–5686.

76 T. Tran-Phu, H. Chen, R. Daiyan, M. Chatti, B. Liu, R. Amal, Y. Liu, D. R. Macfarlane, A. N. Simonov and A. Tricoli,

© 2025 The Author(s). Published by the Royal Society of Chemistry

Open Access Article. Published on 05 February 2025. Downloaded on 2/13/2026 4:26:31 AM. This article is licensed under a Creative Commons Attribution-NonCommercial 3.0 Unported Licence.

Nanoscale TiO_2 Coatings Improve the Stability of an Earth-Abundant Cobalt Oxide Catalyst during Acidic Water Oxidation, *ACS Appl. Mater. Interfaces*, 2022, **14**, 33130–33140.

77 M. Musiani, Anodic deposition of PbO_2/Co_3O_4 composites and their use as electrodes for oxygen evolution reaction, *Chem. Commun.*, 1996, **21**, 2403–2404.

78 G. S. Rocha, A. L. Silva, L. P. C. Silva, F. B. Passos and N. M. F. Carvalho, Improved Activity of PdO Supported over Co_3O_4 in the Electrocatalytic Oxygen Evolution Reaction in a Wide pH Range, *Energy Fuels*, 2022, **36**, 12719–12728.

79 T. Niyitanga and H. Kim, Reduced graphene oxide supported zinc/cobalt oxide nanoparticles as highly efficient electrocatalyst for oxygen evolution reaction, *Inorg. Chim. Acta*, 2022, **539**, 121008.

80 B. Rodríguez-García, Á. Reyes-Carmona, I. Jiménez-Morales, M. Blasco-Ahicart, S. Cavaliere, M. Dupont, D. Jones, J. Rozière, J. R. Galán-Mascarós and F. Jaouen, Cobalt hexacyanoferrate supported on Sb-doped SnO_2 as a non-noble catalyst for oxygen evolution in acidic medium, *Sustainable Energy Fuels*, 2018, **2**, 589–597.

81 X. M. C. Ta, T. Trân-Phú, J. A. Yuwono, T. K. A. Nguyen, A. D. Bui, T. N. Truong, L. C. Chang, E. Magnano, R. Daiyan, A. N. Simonov and A. Tricoli, Optimal Coatings of Co_3O_4 Anodes for Acidic Water Electrooxidation, *Small*, 2023, **20**, 2304650.

82 Q. W. Lai, V. Vediyappan, K. F. Aguey-Zinsou and H. Matsumoto, One-Step Synthesis of Carbon-Protected CoO Nanoparticles toward Long-Term Water Oxidation in Acidic Media, *Adv. Energy Sustainability Res.*, 2021, **2**, 2100086.

83 X. Yang, H. Li, A.-Y. Lu, S. Min, Z. Idriss, M. N. Hedhili, K.-W. Huang, H. Idriss and L.-J. Li, Highly acid-durable carbon coated Co_3O_4 nanoarrays as efficient oxygen evolution electrocatalysts, *Nano Energy*, 2016, **25**, 42–50.

84 J. Yu, F. A. Garces-Pineda, J. Gonzalez-Cobos, M. Pena-Diaz, C. Rogero, S. Gimenez, M. C. Spadaro, J. Arbiol, S. Barja and J. R. Galan-Mascaros, Sustainable oxygen evolution electrocatalysis in aqueous 1 M H_2SO_4 with earth abundant nanostructured Co_3O_4, *Nat. Commun.*, 2022, **13**, 4341.

85 Y.-X. Yeh, C.-C. Cheng, P.-S. Jhu, S.-H. Lin, P.-W. Chen and S.-Y. Lu, Core-shell FTO@Co_3O_4 nanoparticles as active and stable anode catalysts for acidic oxygen evolution reaction and proton exchange membrane water electrolysis, *J. Mater. Chem. A*, 2023, **11**, 3399–3407.

86 A. Yu, M. H. Kim, C. Lee and Y. Lee, Structural transformation between rutile and spinel crystal lattices in Ru-Co binary oxide nanotubes: enhanced electron transfer kinetics for the oxygen evolution reaction, *Nanoscale*, 2021, **13**, 13776–13785.

87 S. Anantharaj, K. Karthick and S. Kundu, Spinel Cobalt Titanium Binary Oxide as an All-Non-Precious Water Oxidation Electrocatalyst in Acid, *Inorg. Chem.*, 2019, **58**, 8570–8576.

88 A. Babaei and M. Rezaei, Development of a highly stable and active non-precious anode electrocatalyst for oxygen evolution reaction in acidic medium based on nickel and cobalt-containing antimony oxide, *J. Electroanal. Chem.*, 2023, **935**, 117319.

89 M. Chatti, J. L. Gardiner, M. Fournier, B. Johannessen, T. Williams, T. R. Gengenbach, N. Pai, C. Nguyen, D. R. MacFarlane, R. K. Hocking and A. N. Simonov, Intrinsically stable in situ generated electrocatalyst for long-term oxidation of acidic water at up to 80 °C, *Nat. Catal.*, 2019, **2**, 457–465.

90 M. Huynh, T. Ozel, C. Liu, E. C. Lau and D. G. Nocera, Design of template-stabilized active and earth-abundant oxygen evolution catalysts in acid, *Chem. Sci.*, 2017, **8**, 4779–4794.

91 Y. Wang, H. Zhao, Y. Guo, J. Wu, X. Lu and X. Tang, Pyrochlore-type cobalt and manganese antimonate electrocatalysts with excellent activity and stability for OER in acidic solution, *Nanoscale*, 2023, **15**, 9413–9422.

92 T. A. Evans and K. S. Choi, Electrochemical Synthesis and Investigation of Stoichiometric, Phase-Pure CoSbO and MnSbO Electrodes for the Oxygen Evolution Reaction in Acidic Media, *ACS Appl. Energy Mater.*, 2020, **3**, 5563–5571.

93 B. Liu, Y. Sun, L. Liu, S. Xu and X. Yan, Advances in Manganese-Based Oxides Cathodic Electrocatalysts for Li-Air Batteries, *Adv. Funct. Mater.*, 2018, **28**, 1704973.

94 A. Bergmann, I. Zaharieva, H. Dau and P. Strasser, Electrochemical water splitting by layered and 3D cross-linked manganese oxides: correlating structural motifs and catalytic activity, *Energy Environ. Sci.*, 2013, **6**, 2745.

95 T. Hayashi, N. Bonnet-Mercier, A. Yamaguchi, K. Suetsugu and R. Nakamura, Electrochemical characterization of manganese oxides as a water oxidation catalyst in proton exchange membrane electrolysers, *R. Soc. Open Sci.*, 2019, **6**, 190122.

96 A. Li, H. Ooka, N. Bonnet, T. Hayashi, Y. Sun, Q. Jiang, C. Li, H. Han and R. Nakamura, Stable Potential Windows for Long-Term Electrocatalysis by Manganese Oxides Under Acidic Conditions, *Angew. Chem., Int. Ed.*, 2019, **58**, 5054–5058.

97 S. Pan, H. Li, D. Liu, R. Huang, X. Pan, D. Ren, J. Li, M. Shakouri, Q. Zhang, M. Wang, C. Wei, L. Mai, B. Zhang, Y. Zhao, Z. Wang, M. Graetzel and X. Zhang, Efficient and stable noble-meta-free catalyst for acidic water oxidation, *Nat. Commun.*, 2022, **13**, 2294.

98 S. Kong, A. Li, J. Long, K. Adachi, D. Hashizume, Q. Jiang, K. Fushimi, H. Ooka, J. Xiao and R. Nakamura, Acid-stable manganese oxides for proton exchange membrane water electrolysis, *Nat. Catal.*, 2024, **7**, 252–261.

99 G. Yan, Y. Lian, Y. Gu, C. Yang, H. Sun, Q. Mu, Q. Li, W. Zhu, X. Zheng, M. Chen, J. Zhu, Z. Deng and Y. Peng, Phase and Morphology Transformation of MnO_2 Induced by Ionic Liquids toward Efficient Water Oxidation, *ACS Catal.*, 2018, **8**, 10137–10147.

100 M. Huynh, C. Shi, S. J. L. Billinge and D. G. Nocera, Nature of Activated Manganese Oxide for Oxygen Evolution, *J. Am. Chem. Soc.*, 2015, **137**, 14887–14904.

Open Access Article. Published on 05 February 2025. Downloaded on 2/13/2026 4:26:31 AM. This article is licensed under a Creative Commons Attribution-NonCommercial 3.0 Unported Licence.

101 Y.-F. Li and Z.-P. Liu, Active Site Revealed for Water Oxidation on Electrochemically Induced δ-MnO_2: Role of Spinel-to-Layer Phase Transition, *J. Am. Chem. Soc.*, 2018, **140**, 1783–1792.

102 S. D. Ghadge, O. I. Velikokhatnyi, M. K. Datta, P. M. Shanthi, S. Tan and P. N. Kumta, Computational and Experimental Study of Fluorine Doped $(Mn_{1-x}Nb_x)O_2$ Nanorod Electrocatalysts for Acid-Mediated Oxygen Evolution Reaction, *ACS Appl. Energy Mater.*, 2019, **3**, 541–557.

103 P. P. Patel, M. K. Datta, O. I. Velikokhatnyi, R. Kuruba, K. Damodaran, P. Jampani, B. Gattu, P. M. Shanthi, S. S. Damle and P. N. Kumta, Noble metal-free bifunctional oxygen evolution and oxygen reduction acidic media electro-catalysts, *Sci. Rep.*, 2016, **6**, 28367.

104 K. Lemoine, Z. Gohari-Bajestani, R. Moury, A. Terry, A. Guiet, J.-M. Grenèche, A. Hémon-Ribaud, N. Heidary, V. Maisonneuve, N. Kornienko and J. Lhoste, Amorphous Iron-Manganese Oxyfluorides, Promising Catalysts for Oxygen Evolution Reaction under Acidic Media, *ACS Appl. Energy Mater.*, 2021, **4**, 1173–1181.

105 Y. Li, L. Jiang, F. Liu, J. Li and Y. Liu, Novel phosphorus-doped PbO_2-MnO_2 bicontinuous electrodes for oxygen evolution reaction, *RSC Adv.*, 2014, **4**, 24020–24028.

106 Y. Lai, Y. Li, L. Jiang, W. Xu, X. Lv, J. Li and Y. Liu, Electrochemical behaviors of co-deposited Pb/Pb-MnO_2 composite anode in sulfuric acid solution-Tafel and EIS investigations, *J. Electroanal. Chem.*, 2012, **671**, 16–23.

107 R. Frydendal, E. A. Paoli, I. Chorkendorff, J. Rossmeisl and I. E. L. Stephens, Toward an Active and Stable Catalyst for Oxygen Evolution in Acidic Media: Ti-Stabilized MnO_2, *Adv. Energy Mater.*, 2015, **5**, 1500991.

108 Z. Zand, M. R. Mohammadi, A. S. Sologubenko, S. Handschin, R. Bagheri, P. Chernev, Z. Song, H. Dau and M. M. Najafpour, Oxygen Evolution Reaction by Silicate-Stabilized Manganese Oxide, *ACS Appl. Energy Mater.*, 2023, **6**, 1702–1713.

109 I. A. Moreno-Hernandez, C. A. MacFarland, C. G. Read, K. M. Papadantonakis, B. S. Brunschwig and N. S. Lewis, Crystalline nickel manganese antimonate as a stable water-oxidation catalyst in aqueous 1.0 M H_2SO_4, *Energy Environ. Sci.*, 2017, **10**, 2103–2108.

110 L. Zhou, A. Shinde, J. H. Montoya, A. Singh, S. Gul, J. Yano, Y. Ye, E. J. Crumlin, M. H. Richter, J. K. Cooper, H. S. Stein, J. A. Haber, K. A. Persson and J. M. Gregoire, Rutile Alloys in the Mn-Sb-O System Stabilize Mn^{3+} To Enable Oxygen Evolution in Strong Acid, *ACS Catal.*, 2018, **8**, 10938–10948.

111 Z. P. Ifkovits, J. M. Evans, P. A. Kempler, M. B. Morla, K. H. Pham, J. A. Dowling, A. I. Carim and N. S. Lewis, Powdered $Mn_ySb_{1-y}O_x$ Catalysts for Cerium-Mediated Oxygen Evolution in Acidic Environments, *ACS Energy Lett.*, 2022, **7**, 4258–4264.

112 N. Han, K. R. Yang, Z. Lu, Y. Li, W. Xu, T. Gao, Z. Cai, Y. Zhang, V. S. Batista, W. Liu and X. Sun, Nitrogen-doped tungsten carbide nanoarray as an efficient bifunctional electrocatalyst for water splitting in acid, *Nat. Commun.*, 2018, **9**, 924.

113 C. Lei, H. Chen, J. Cao, J. Yang, M. Qiu, Y. Xia, C. Yuan, B. Yang, Z. Li, X. Zhang, L. Lei, J. Abbott, Y. Zhong, X. Xia, G. Wu, Q. He and Y. Hou, FeN_4 Sites Embedded into Carbon Nanofiber Integrated with Electrochemically Exfoliated Graphene for Oxygen Evolution in Acidic Medium, *Adv. Energy Mater.*, 2018, **8**, 1801912.

114 Z. Liu, H. Tan, D. Liu, X. Liu, J. Xin, J. Xie, M. Zhao, L. Song, L. Dai and H. Liu, Promotion of Overall Water Splitting Activity Over a Wide pH Range by Interfacial Electrical Effects of Metallic NiCo-nitrides Nanoparticle/$NiCo_2O_4$ Nanoflake/graphite Fibers, *Advanced Science*, 2019, **6**, 1801829.

115 R. Ram, L. Xia, H. Benzidi, A. Guha, V. Golovanova, A. Garzon Manjon, D. Llorens Rauret, P. Sanz Berman, M. Dimitropoulos, B. Mundet, E. Pastor, V. Celorrio, C. A. Mesa, A. M. Das, A. Pinilla-Sanchez, S. Gimenez, J. Arbiol, N. Lopez and F. P. Garcia de Arquer, Water-hydroxide trapping in cobalt tungstate for proton exchange membrane water electrolysis, *Science*, 2024, **384**, 1373–1380.

116 J. Wu, M. Liu, K. Chatterjee, K. P. Hackenberg, J. Shen, X. Zou, Y. Yan, J. Gu, Y. Yang, J. Lou and P. M. Ajayan, Exfoliated 2D Transition Metal Disulfides for Enhanced Electrocatalysis of Oxygen Evolution Reaction in Acidic Medium, *Adv. Mater. Interfaces*, 2016, **3**, 1500669.

117 Q. Hu, G. Li, X. Liu, B. Zhu, G. Li, L. Fan, X. Chai, Q. Zhang, J. Liu and C. He, Coupling pentlandite nanoparticles and dual-doped carbon networks to yield efficient and stable electrocatalysts for acid water oxidation, *J. Mater. Chem. A*, 2019, **7**, 461–468.

118 M. Liu, Z. Sun, S. Li, X. Nie, Y. Liu, E. Wang and Z. Zhao, Hierarchical superhydrophilic/superaerophobic CoMnP/Ni_2P nanosheet-based microplate arrays for enhanced overall water splitting, *J. Mater. Chem. A*, 2021, **9**, 22129–22139.

119 J. T. Arens, M. Blasco-Ahicart, K. Azmani, J. Soriano-López, A. García-Eguizábal, J. M. Poblet and J. R. Galan-Mascaros, Water oxidation electrocatalysis in acidic media with Co-containing polyoxometalates, *J. Catal.*, 2020, **389**, 345–351.

120 X.-B. Han, D.-X. Wang, E. Gracia-Espino, Y.-H. Luo, Y.-Z. Tan, D.-F. Lu, Y.-G. Li, T. Wågberg, E.-B. Wang and L.-S. Zheng, Fe-substituted cobalt-phosphate polyoxometalates as enhanced oxygen evolution catalysts in acidic media, *Chin. J. Catal.*, 2020, **41**, 853–857.

121 L. G. Bloor, P. I. Molina, M. D. Symes and L. Cronin, Low pH Electrolytic Water Splitting Using Earth-Abundant Metastable Catalysts That Self-Assemble in Situ, *J. Am. Chem. Soc.*, 2014, **136**, 3304–3311.

122 H. Liu, X. Peng, X. Liu, G. Qi and J. Luo, Porous Mn-Doped FeP/$Co_3(PO_4)_2$ Nanosheets as Efficient Electrocatalysts for Overall Water Splitting in a Wide pH Range, *ChemSusChem*, 2019, **12**, 1334–1341.

123 J. S. Mondschein, K. Kumar, C. F. Holder, K. Seth, H. Kim and R. E. Schaak, Intermetallic Ni(2)Ta Electrocatalyst for the Oxygen Evolution Reaction in Highly Acidic Electrolytes, *Inorg. Chem.*, 2018, **57**, 6010–6015.

© 2025 The Author(s). Published by the Royal Society of Chemistry

Open Access Article. Published on 05 February 2025. Downloaded on 2/13/2026 4:26:31 AM.
This article is licensed under a Creative Commons Attribution-NonCommercial 3.0 Unported Licence.

124 B. Shen, Y. He, Z. He, Z. Wang, Y. Jiang and H. Gao, Porous Fe(5)Si(3) intermetallic anode for the oxygen evolution reaction in acidic electrolytes, *J. Colloid Interface Sci.*, 2022, **605**, 637–647.

125 W. Li, B. Shen, J. Kang, Z. Wang and Y. He, Oxygen evolution and corrosion behaviours of the porous Mn5Si3 electrode in sulfuric acid, *Mater. Res. Express*, 2019, **6**, 085542.

126 Z. Wang, Y. Jiang, L. Feng, Z. He, X. Kang, L. Yu, Y. He, Z. Qin, Q. Zhao, Y. Qiu and H. Gao, Synthesis and study of TiMn2 intermetallic compound anode materials with different structures for zinc electrowinning, *Intermetallics*, 2023, **161**, 107989.

127 M. W. Kanan and D. G. Nocera, In situ formation of an oxygen-evolving catalyst in neutral water containing phosphate and Co^{2+}, *Science*, 2008, **321**, 1072–1075.

128 Y. Wang, Y. Zou, L. Tao, Y. Wang, G. Huang, S. Du and S. Wang, Rational design of three-phase interfaces for electrocatalysis, *Nano Res.*, 2019, **12**, 2055–2066.

129 C. Yang, N. Han, Y. Wang, X.-Z. Yuan, J. Xu, H. Huang, J. Fan, H. Li and H. Wang, A Novel Approach to Fabricate Membrane Electrode Assembly by Directly Coating the Nafion Ionomer on Catalyst Layers for Proton-Exchange Membrane Fuel Cells, *ACS Sustain. Chem. Eng.*, 2020, **8**, 9803–9812.